

Deciphering phenylalanine-derived salicylic acid biosynthesis in plants

<https://doi.org/10.1038/s41586-025-09280-9>

Received: 8 September 2024

Accepted: 12 June 2025

Published online: 23 July 2025

Open access

 Check for updates

Yukang Wang^{1,2,12}, Shuyan Song^{1,2,12}, Wenzuan Zhang^{3,12}, Qianwen Deng^{1,2}, Yanlei Feng^{1,2}, Mei Tao⁴, Mengna Kang¹, Qi Zhang¹, Lijia Yang¹, Xinyu Wang¹, Changan Zhu³, Xiaowen Wang^{1,2}, Wanxin Zhu^{1,2}, Yixiao Zhu⁴, Pengfei Cao⁵, Jia Chen⁶, Jinzheng Pan⁶, Shan Feng⁶, Xianyan Chen⁷, Huaxin Dai⁸, Shiyong Song¹, Jinghua Yang³, Tianlun Zhao¹, Fangbin Cao¹, Zeng Tao¹, Xingxing Shen⁴, Robert L. Last^{9,10}, Jianping Hu^{5,10}, Jingquan Yu^{3,11}, Pengxiang Fan^{3,11} & Ronghui Pan^{1,2}✉

Salicylic acid (SA) is a ubiquitous plant hormone with a long history in human civilization^{1,2}. Because of the central role of SA in orchestrating plant pathogen defence, understanding SA biosynthesis is fundamental to plant immunity research and crop improvement. Isochorismate-derived SA biosynthesis has been well defined in *Arabidopsis*. However, increasing evidence suggests a crucial function for phenylalanine-derived SA biosynthesis in many other plant species¹. Here we reveal the phenylalanine-derived SA biosynthetic pathway in rice by identifying three dedicated enzymes – peroxisomal benzoyl-CoA:benzyl alcohol benzoyltransferase (BEBT), the endoplasmic reticulum-associated cytochrome P450 enzyme benzylbenzoate hydroxylase (BBH), and cytosolic benzylsalicylate esterase (BSE) that sequentially convert benzoyl-CoA to benzylbenzoate, benzylsalicylate and SA. The pathogen-induced gene expression pattern and SA biosynthetic functions of this triple-enzyme module are conserved in diverse plants. This work fills a major knowledge gap in the biosynthesis of a key plant defence hormone, establishing a foundation for new strategies to create disease-resistant crops.

The biological effects of SA have been exploited in herbal medicine for more than 4,000 years^{1,2}. In the eighteenth century, SA was isolated from willow and developed into aspirin³. SA is produced in different amounts and with varying organ distribution across the plant kingdom^{4,5}, and best known for its central role in plant immune response^{1,2}. SA also has documented roles in other aspects of plant biology, such as abiotic stress response, development and root microbiome assembly^{6–8}.

In *Arabidopsis*, SA biosynthesis occurs predominantly through the isochorismate synthase (ICS) route^{9–11} (Extended Data Fig. 1). *ICS* gene silencing reduced SA accumulation in the leaves of barley (*Hordeum vulgare*), soybean (*Glycine max*) and wheat (*Triticum aestivum*)^{12–14}. However, disruption of *ICS* in *Aegilops variabilis* roots or barley leaves during pathogen infection^{15,16}, or in *Chlamydomonas reinhardtii*¹⁷ does not reduce the amount of SA. Similarly, rice (*Oryza sativa*), which has high levels of basal SA in leaves, maintains normal SA levels in *ICS*-null mutants¹⁸. Furthermore, *ICS* disruption often severely impairs photosynthesis and growth^{16,18,19}, potentially affecting SA-related metabolism indirectly.

Isotope tracking studies in various plant lineages support the existence of an alternative phenylalanine-derived SA biosynthetic

pathway (Extended Data Fig. 2a). This route shares common precursors with phenylpropanoid metabolism, beginning with phenylalanine ammonia lyase (PAL), which converts phenylalanine to cinnamic acid, followed by cinnamoyl-coenzyme A (cinnamoyl-CoA) formation and β-oxidation in peroxisomes^{1,2} (Extended Data Fig. 1). Benzoic acid (BA) has been proposed to be the product of cinnamic acid β-oxidation and the immediate precursor for SA biosynthesis^{1,2} (Extended Data Fig. 1). Despite these early findings, the final steps specifically dedicated to SA biosynthesis remain unresolved.

Phenylalanine, cinnamic acid and BA serve as precursors for multiple metabolite classes beyond SA (Extended Data Fig. 1), including phenylpropanoids such as lignin, flavonoids and coumarins²⁰, and BA derivatives such as benzyl alcohol and benzyl aldehyde²¹ (Extended Data Fig. 1). Additionally, β-oxidation enzymes, including abnormal inflorescence meristem1 (AIM1), also participate in synthesizing other hormones, such as jasmonic acid and indole-3-acetic acid and central metabolites, such as acetyl-CoA and ubiquinone²². Disrupting PALs or AIM1 often leads to pleiotropic effects and even lethality^{5,23–25}, complicating functional studies of SA production and signalling⁵. Thus, identifying the final and more

¹State Key Laboratory of Rice Biology and Breeding, Zhejiang Key Laboratory of Crop Germplasm Innovation and Utilization, College of Agriculture and Biotechnology, Zhejiang University, Hangzhou, China. ²Zhejiang Key Laboratory of Intelligent Manufacturing for Functional Chemicals, ZJU-Hangzhou Global Scientific and Technological Innovation Center, Zhejiang University, Hangzhou, China. ³Department of Horticulture, College of Agriculture and Biotechnology, Zhejiang University, Hangzhou, China. ⁴Key Laboratory of Biology of Crop Pathogens and Insects of Zhejiang Province, College of Agriculture and Biotechnology, Zhejiang University, Hangzhou, China. ⁵Michigan State University—Department of Energy Plant Research Laboratory, Michigan State University, East Lansing, MI, USA. ⁶Mass Spectrometry and Metabolomics Core Facility, The Biomedical Research Core Facility, Westlake University, Hangzhou, China. ⁷Material Scientific Cores, Zhejiang Laboratory, Hangzhou, China. ⁸Beijing Life Science Academy, Changping, Beijing, China. ⁹Department of Biochemistry and Molecular Biology, Michigan State University, East Lansing, MI, USA. ¹⁰Department of Plant Biology, Michigan State University, East Lansing, MI, USA. ¹¹Key Laboratory of Horticultural Plants Growth and Development, Agricultural Ministry of China, Hangzhou, China. ¹²These authors contributed equally: Yukang Wang, Shuyan Song, Wenzuan Zhang. ✉e-mail: pxfan@zju.edu.cn; panr@zju.edu.cn

specific SA biosynthetic steps in the phenylalanine-derived pathway is crucial.

Despite isotope-based evidence implicating SA biosynthesis from phenylalanine, cinnamic acid and BA (Extended Data Fig. 2a), how SA is ultimately formed remained unclear. Cytochrome P450 (CYP) inhibitors block SA biosynthesis in many plants (Extended Data Fig. 2b), prompting the proposal of a CYP that hydroxylates BA to SA^{26,27}. However, extensive searches have not been able to identify such a CYP. Here we closed this long-standing gap by identifying a triple-enzyme cascade dedicated to SA biosynthesis in rice. Through gene co-expression, protein localization, and genetic and biochemical analyses, we show that the peroxisomal BEBT, the endoplasmic reticulum-associated CYP BBH and the cytosolic BSE function sequentially to generate SA. We also demonstrate the functional conservation of these enzymes in diverse plant species.

BEBT converts benzoyl-CoA to benzylbenzoate

We recently identified the peroxisome-localized cinnamate:CoA ligases (CNLs) as essential enzymes in rice SA biosynthesis, which activate cinnamic acid to cinnamoyl-CoA for peroxisomal β -oxidation^{5,28}. Through β -oxidation, cinnamoyl-CoA is converted to benzoyl-CoA in peroxisomes^{22,29,30} (Extended Data Fig. 1). *OsCNL* double mutants (later referred to as *cnl*) exhibit an approximately 83% decrease of benzoyl-CoA (Fig. 1a) and approximately 51% decrease of BA (Fig. 1b) in leaves. The partial reduction of BA is consistent with the existence of multiple BA-forming pathways in plants²¹.

We hypothesized that the next key step in SA biosynthesis following benzoyl-CoA formation might also occur in peroxisomes. To identify candidate enzymes for this step, we performed a co-expression analysis of *OsCNL1*, whose gene product has a more specialized role than PAL and AIM1 in SA biosynthesis⁵ and whose expression is strongly up-regulated by SA-inducing stimuli^{28,31}. Among the co-expressed genes that encode proteins containing peroxisome-targeting signal (PTS) peptides³², *Os10g0503300*, which encodes a clade-V BAHD acyltransferase³³ and contains a C-terminal type-1PTS (PTS1) (Extended Data Fig. 3a), showed the highest co-expression value (Fig. 1c).

Phylogenetic analysis placed *Os10g0503300* in a subfamily comprising enzymes with verified benzoyl-CoA:benzyl alcohol benzoyl-transferase (BEBT) activities^{34–36}, including those from *Clarkia breweri*, *Populus trichocarpa* and *Petunia hybrida* (Extended Data Figs. 3a and 4a). Thus, *Os10g0503300* was subsequently named OsBEBT. A notable member of this subfamily is the tobacco (*Nicotiana tabacum*) hypersensitivity-related gene 201 (NtHSR201) protein, whose gene silencing compromised pathogen elicitor-induced SA biosynthesis³⁷. Although its biochemical function has not been characterized, NtHSR201 was further suggested to function cooperatively with peroxisomal β -oxidation based on transient co-overexpression assays³⁸ and was recently shown to be peroxisomal³⁹. Consistent with the presence of PTS1 peptides in all of these BEBT homologues (Extended Data Fig. 3a), transient co-expression of the yellow fluorescent protein (YFP) fusion protein YFP–OsBEBT with a peroxisome cyan fluorescent protein marker (CFP–SKL) confirmed the peroxisomal localization of OsBEBT in *Nicotiana benthamiana* epidermal cells (Fig. 1d). We also measured OsBEBT's enzyme activity using purified recombinant OsBEBT proteins expressed in *Escherichia coli* (Extended Data Fig. 3b). As expected, OsBEBT exhibited highest catalytic efficiency (lowest Michaelis constant (K_m) and highest k_{cat}/K_m , where k_{cat} is the catalytic constant) toward benzoyl-CoA when benzyl alcohol was used as the acyl acceptor substrate (Fig. 1e and Extended Data Fig. 3c), compared with using *trans*-cinnamyl alcohol, vanillic alcohol (3-methoxy-4-hydroxy benzyl alcohol) and isovanillyl alcohol (4-methoxy-3-hydroxy benzyl alcohol) as the acyl acceptor (Extended Data Fig. 3c). These kinetic parameters indicate that OsBEBT preferentially catalyses the formation of benzylbenzoate by transferring the benzoyl group from benzoyl-CoA to benzyl alcohol.

To determine whether OsBEBT is required for SA biosynthesis in rice, we obtained two mutants, *bebt-1* and *bebt-2*, both of which contain frameshift mutations (Extended Data Fig. 3d). In our growth conditions, wild-type rice leaf tissue accumulates SA approximately two weeks after germination (Extended Data Fig. 3e). However, *bebt* leaves exhibited a near-complete loss of SA in both two-week-old and 5-day-old plants, a phenotype similar to that of the *cnl* mutant (Fig. 1f and Extended Data Fig. 3f), demonstrating the essential role of OsBEBT in SA biosynthesis.

Informed by the biochemical activity of OsBEBT (Fig. 1e), we next performed metabolite analyses of mutants to determine *in vivo* whether OsBEBT consumes benzoyl-CoA and produces benzylbenzoate. Indeed, benzoyl-CoA significantly accumulated in *bebt* (Fig. 1g), in contrast to the strong reduction in *cnl* (Fig. 1a), supporting benzoyl-CoA as an intermediate metabolite between OsCNL and OsBEBT. Additionally, benzylbenzoate markedly decreased to undetectable levels in both *bebt* and *cnl* mutants (Fig. 1h), consistent with OsCNL being a component upstream of OsBEBT.

To establish the importance of benzylbenzoate in SA biosynthesis and test whether benzylbenzoate deficiency directly limits SA biosynthesis in *bebt* and *cnl* plants, we performed chemical complementation assays. Exogenous benzylbenzoate successfully restored SA levels in both mutants (Extended Data Fig. 3f). Together, our *in vivo* and *in vitro* findings established OsBEBT as a key enzyme in the conversion of peroxisomal benzoyl-CoA to benzylbenzoate.

BA is not the direct precursor for SA

The finding that β -oxidation-derived benzoyl-CoA is utilized by OsBEBT prompted us to check whether BA is generated downstream of OsBEBT. BA was proposed to be the direct precursor of SA and hypothesized to be converted to SA by a BA 2-hydroxylase (BA2H)^{1,2}. Rice *cnl* and *aim1* mutants showed reduced BA levels, which can be restored by exogenous BA^{5,23,28,40}. These observations indicated that BA is a downstream product of cinnamoyl-CoA β -oxidation and that exogenously added BA can be utilized for SA biosynthesis, but did not establish whether BA is the direct hydroxylation substrate for SA biosynthesis.

Notably, BA was strongly increased in *bebt* plants (Fig. 2a), in marked contrast to the decreased BA in *cnl* (Fig. 1b) and *aim1* mutants^{5,23,28,40}. Thus, BA shares the same pattern with benzoyl-CoA by accumulating in *bebt* and decreasing in *cnl* mutants (Fig. 1a,g), suggesting that BA, just like benzoyl-CoA, is not a downstream metabolite of OsBEBT. More importantly, exogenous BA did not restore SA levels in the *bebt* mutant (Fig. 2b), again in contrast to the partial to full complementation effect of BA in *cnl* and *aim1*^{5,23,28,40}. Thus, exogenous BA contributes to SA biosynthesis upstream of OsBEBT instead of acting as the direct precursor for SA.

To investigate how exogenous BA can contribute to SA biosynthesis, we used stable isotope tracking experiments. In wild-type ZH11 rice, labelled BA was metabolized to benzoyl-CoA, benzylbenzoate and SA (Fig. 2c–f). However, this conversion was abolished in the *bebt* mutant (Fig. 2d–f), confirming that the contribution of exogenous BA to SA biosynthesis requires OsBEBT. Consistently, we also detected isotope-labelled benzoyl-CoA—the donor substrate of OsBEBT—to be more highly accumulated in *bebt* than in wild-type rice (Fig. 2c). These data suggested that exogenous BA is first converted to benzoyl-CoA and then utilized by OsBEBT; thus, BA is not the direct precursor of SA.

Additional support of this conclusion came from the analysis of the rice orthologues of *P. hybrida* thioesterases (PhTE1 and PhTE2), which hydrolyse benzoyl-CoA to BA in peroxisomes⁴¹ (Extended Data Fig. 5a,b). Rice OsTE1 and OsTE2 showed PTS1-dependent peroxisomal localization and benzoyl-CoA hydrolase activity (Extended Data Fig. 5c,d). Notably, *te1 te2* double mutants showed increased rather than decreased levels of SA and its derivative (Extended Data Fig. 5e–g), despite having unchanged levels of BA, benzoyl-CoA and

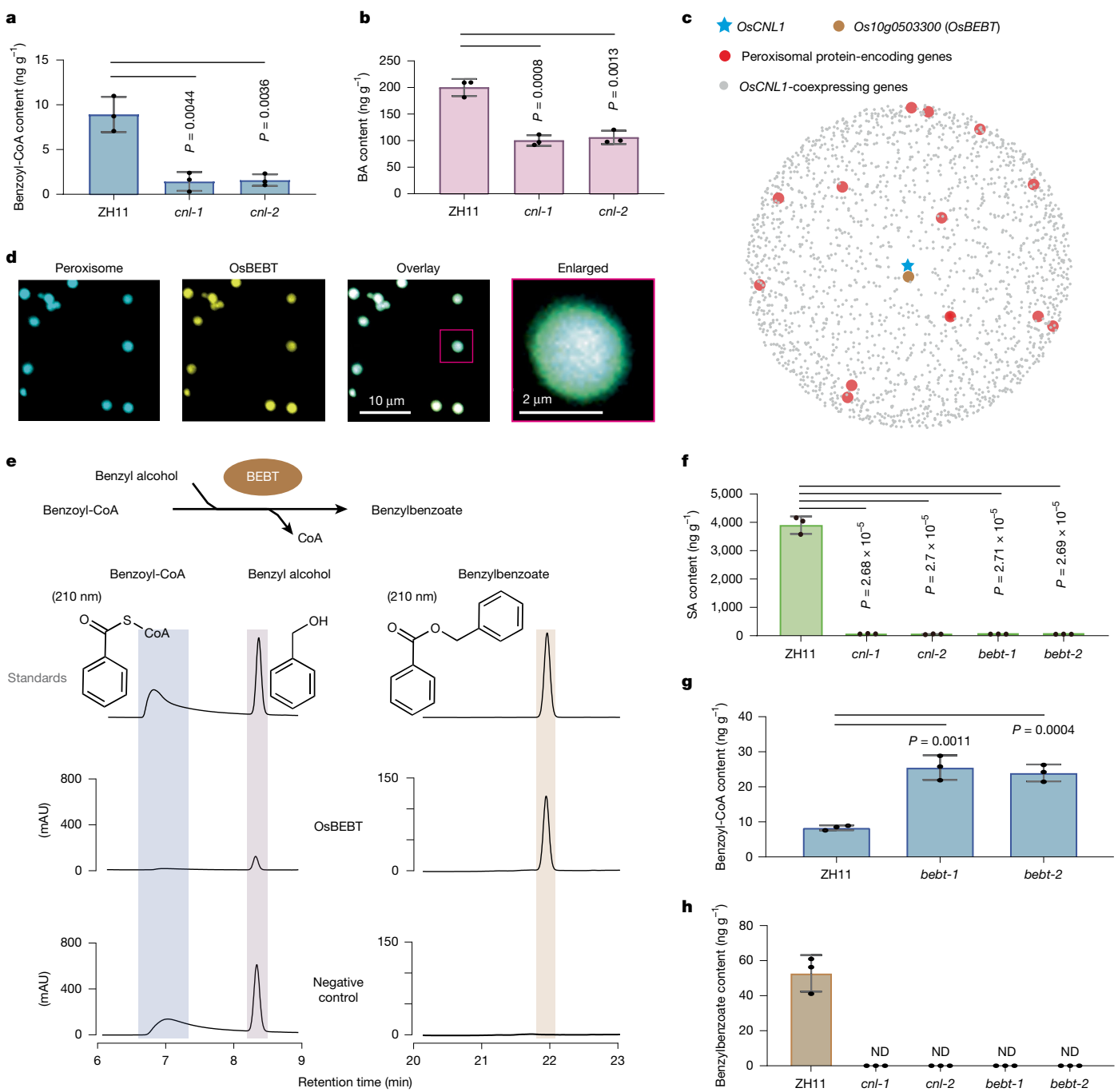


Fig. 1 | Peroxisomal OsBEBT converts benzoyl-CoA to benzylbenzoate. **a, b**, Quantification of benzoyl-CoA (**a**) and BA (**b**) in leaves from two-week-old wild-type (ZH11) and *cnl* mutant rice by liquid chromatography–tandem mass spectrometry (LC–MS/MS) with multiple reaction monitoring (MRM). Values were normalized to fresh weight. Data are mean \pm s.d. ($n = 3$ biologically independent samples). Statistical significance was determined by two-tailed Student's *t*-tests. **c**, Gene co-expression analysis to identify peroxisomal protein-encoding genes that are highly co-expressed with *OsCNL1*. The plot shows the top 2,000 genes that are co-expressed with *OsCNL1*, each represented as a dot (data source: ATTED-II; <https://atted.jp/>). The dot-to-pentagram distance scales inversely with bait gene co-expression strength. **d**, Subcellular localization of YFP–OsBEBT. Confocal microscopy images show the co-localization of YFP–

OsBEBT and the peroxisome marker CFP–SKL in *N. benthamiana* leaf epidermis. The region outlined in magenta is enlarged and displayed on the right. **e**, High-performance liquid chromatography (HPLC) analysis of purified recombinant OsBEBT proteins incubated with benzoyl-CoA and benzyl alcohol in enzymatic reactions. Heat-inactivated OsBEBT served as the negative control. Chromatographs of absorbance at wavelength 210 nm indicate substrates and products. **f–h**, Metabolite analysis of leaves from two-week-old wild-type (ZH11) and *bebt* and *cnl* mutant rice. SA (**f**), benzoyl-CoA (**g**) and benzylbenzoate (**h**) were quantified by LC–MS/MS with MRM and normalized to fresh weight. Data are mean \pm s.d. ($n = 3$ biologically independent samples). Statistical significance was determined by two-tailed Student's *t*-tests. ND, not determined.

benzylbenzoate (Extended Data Fig. 5h–j). SA accumulation in the *te1 te2* mutants excludes a positive role of OsTE1 and OsTE2 in SA biosynthesis and helps to refute BA as the direct hydroxylation precursor for SA.

BBH is the CYP hydroxylase

CYP monooxygenase inhibitors were reported to prevent SA accumulation in many species (Extended Data Fig. 2b), leading to the suggestion

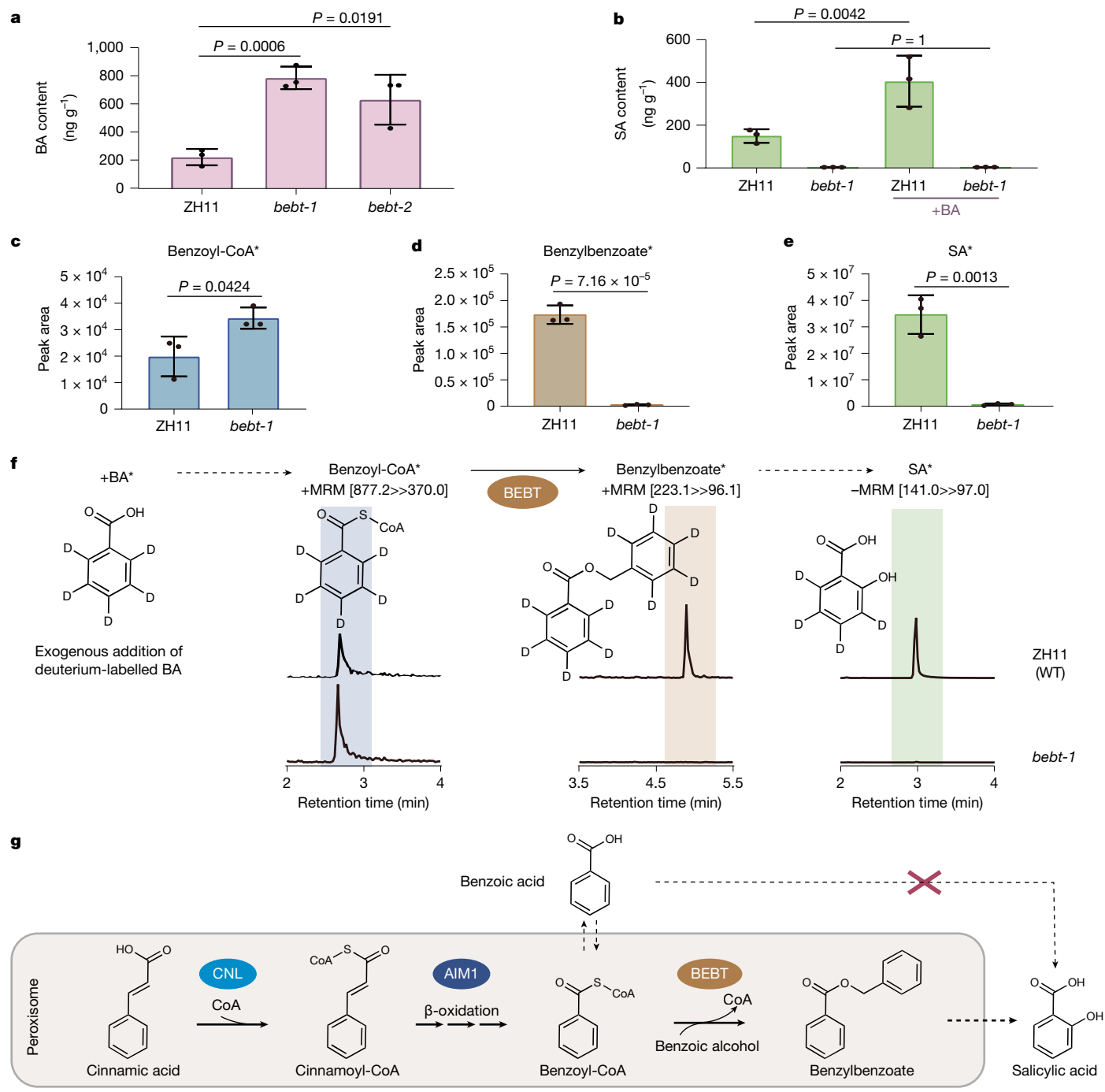


Fig. 2 | BA is not the direct hydroxylation precursor for SA. **a**, BA content in leaves of two-week-old wild-type (ZH11) and *betb* mutant rice, measured by LC-MS/MS with MRM and normalized to fresh weight. Data are mean \pm s.d. ($n = 3$ biologically independent samples). Statistical significance was determined by two-tailed Student's *t*-tests. **b**, SA accumulation in leaves of five-day-old ZH11 and *betb* mutant rice fed with or without BA. SA content was analysed by LC-MS/MS with MRM and normalized to fresh weight. Data are mean \pm s.d. ($n = 3$ biologically independent samples). Statistical significance was determined by one-way ANOVA with post hoc Tukey honest significant difference (HSD) test. **c–e**, Metabolic flux analysis using deuterium-labelled BA in leaves from five-day-old ZH11 and *betb* mutant rice. Metabolites were extracted from equal fresh weights of leaf tissue and analysed by LC-MS/MS with MRM. Signal intensities of labelled benzoyl-CoA (**c**), benzylbenzoate (**d**) and SA (**e**) are presented as

normalized peak areas. Data are mean \pm s.d. ($n = 3$ biologically independent samples). Statistical significance was determined by two-tailed Student's *t*-tests. **(f)** Representative LC-MS chromatograms of deuterium-labelled metabolites detected by MRM. Transitions monitored include: +MRM ($877.2 \rightarrow 370.0$) for deuterium-labelled benzoyl-CoA, +MRM ($223.1 \rightarrow 96.1$) for deuterium-labelled benzylbenzoate and -MRM ($141.0 \rightarrow 97.0$) for deuterium-labelled SA. Peak intensities relative to the highest signal for each compound are shown. **c–f**, Asterisks indicate deuterium-labelled metabolites; + and – denote positive and negative ionization modes, respectively. **g**, Proposed metabolic pathway showing that BA is not directly hydroxylated to SA. Cinnamoyl-CoA is first converted through β -oxidation to benzoyl-CoA and then to benzylbenzoate, the proposed precursor of SA biosynthesis.

that an unidentified BA2H is involved^{26,27}. After excluding BA as the direct hydroxylation precursor of SA, we focused on CYPs as candidates for the next dedicated enzyme after BEBT in SA biosynthesis. Using

Oscnl1-based co-expression analysis, we identified *Osg0441400* as the most strongly co-expressed CYP (Fig. 3a). This protein, later renamed benzylbenzoate hydroxylase (OsBBH), contains an N-terminal

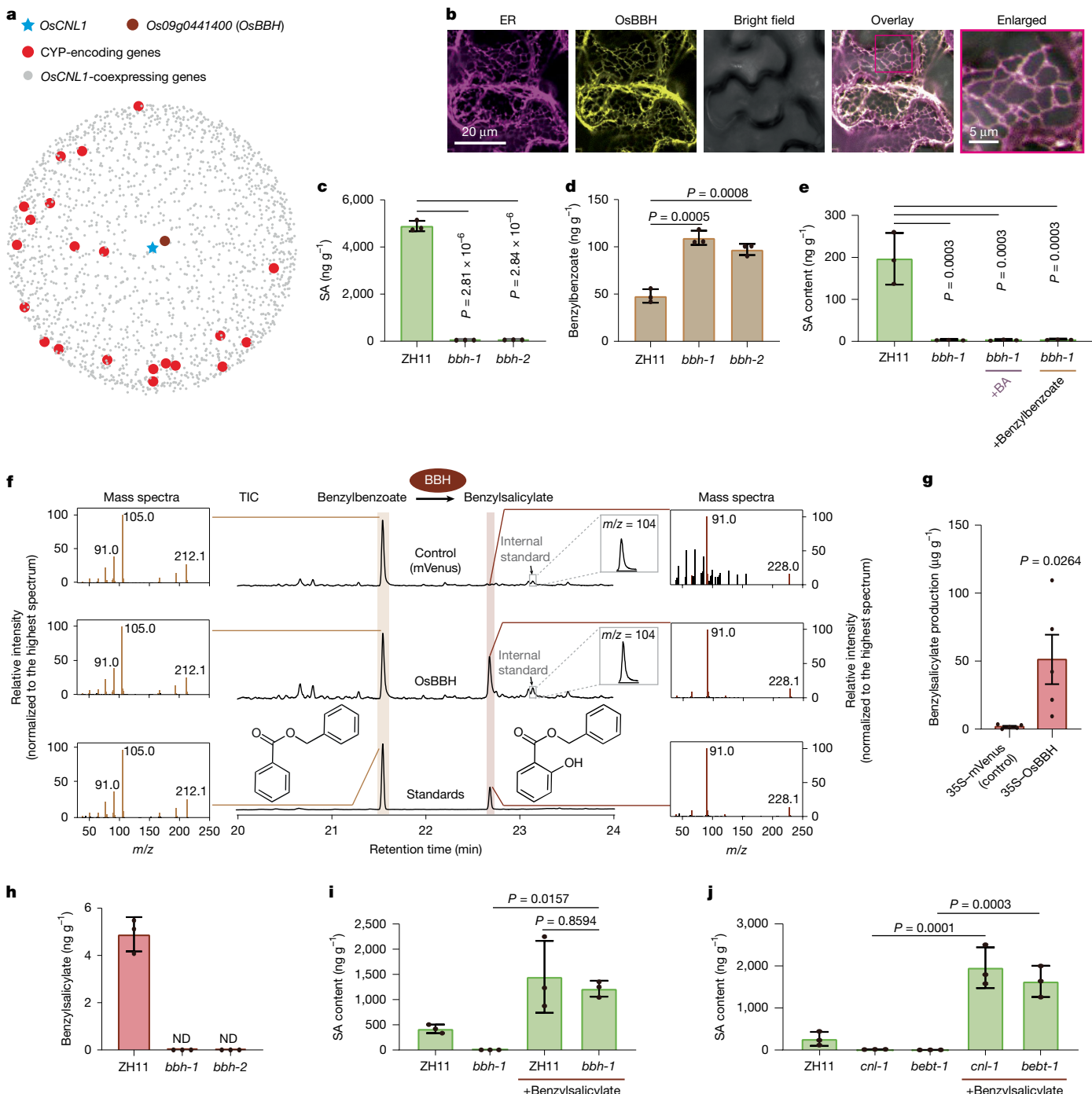


Fig. 3 | The endoplasmic reticulum-localized OsBBH hydroxylates benzylbenzoate. **a**, Co-expression network analysis identifying CYP genes co-expressed with OsCNL1. **b**, Subcellular localization of YFP–OsBBH. Confocal microscopy images show the co-localization of YFP–OsBBH and the endoplasmic reticulum (ER) marker (ER-rk) in *N. benthamiana* leaf epidermis. The region outlined in magenta is enlarged and displayed on the right. **c,d**, Quantification of SA (**c**) and benzylbenzoate (**d**) in leaves from two-week-old rice. Data are mean \pm s.d. ($n = 3$ biologically independent samples). Statistical significance was determined by two-tailed Student's *t*-tests. **e**, SA contents in five-day-old rice *bbh* mutants fed with BA or benzylbenzoate. Data are mean \pm s.d. ($n = 3$ biologically independent samples). Statistical significance was determined by one-way ANOVA with post hoc Tukey HSD test. **f,g**, Functional characterization of OsBBH in *N. benthamiana*. Leaves transiently expressing OsBBH or mVenus (control) were treated with benzylbenzoate. **f**, Gas chromatography–mass spectrometry (GC–MS) analysis showing mass spectra of benzylbenzoate and benzylsalicylate compared to authentic standards. Enlarged chromatograms display $m/z = 104$ with phenethyl phenylacetate as internal standard (indicated by arrow). TIC, total ion chromatogram. **g**, Benzylsalicylate was quantified using extracted ion chromatograms (EIC; $m/z = 228$) normalized to internal standard (EIC $m/z = 104$), and the production was normalized to fresh weight of *N. benthamiana* leaves. Data are mean \pm s.e.m. ($n = 5$ independent experiments). Statistical significance was determined by two-tailed Student's *t*-tests. **h**, Quantification of benzylsalicylate in leaves from two-week-old wild-type and *bbh* mutant rice. Data are mean \pm s.d. ($n = 3$ biologically independent samples). **i,j**, SA content of five-day-old rice *bbh* (**i**), *cnl* and *bebt* (**j**) mutants fed with benzylsalicylate. Data are mean \pm s.d. ($n = 3$ biologically independent samples). Statistical significance was determined by one-way ANOVA with post hoc Tukey HSD test. In **c–e** and **h–j**, metabolites were analysed by LC–MS/MS with MRM and normalized to fresh weight.

benzylsalicylate compared to authentic standards. Enlarged chromatograms display $m/z = 104$ with phenethyl phenylacetate as internal standard (indicated by arrow). TIC, total ion chromatogram. **g**, Benzylsalicylate was quantified using extracted ion chromatograms (EIC; $m/z = 228$) normalized to internal standard (EIC $m/z = 104$), and the production was normalized to fresh weight of *N. benthamiana* leaves. Data are mean \pm s.e.m. ($n = 5$ independent experiments). Statistical significance was determined by two-tailed Student's *t*-tests. **h**, Quantification of benzylsalicylate in leaves from two-week-old wild-type and *bbh* mutant rice. Data are mean \pm s.d. ($n = 3$ biologically independent samples). **i,j**, SA content of five-day-old rice *bbh* (**i**), *cnl* and *bebt* (**j**) mutants fed with benzylsalicylate. Data are mean \pm s.d. ($n = 3$ biologically independent samples). Statistical significance was determined by one-way ANOVA with post hoc Tukey HSD test. In **c–e** and **h–j**, metabolites were analysed by LC–MS/MS with MRM and normalized to fresh weight.

Article

signal peptide for the endomembrane system but lacks peroxisomal targeting signals (Extended Data Fig. 6a). Using the *N. benthamiana* leaf transient gene expression system, we confirmed the endoplasmic reticulum localization of OsBBH-YFP (Fig. 3b and Extended Data Fig. 6b).

To check whether OsBBH is involved in SA biosynthesis in planta, we obtained two frameshift mutant lines, *bbh-1* and *bbh-2* (Extended Data Fig. 6c). Both mutants exhibited a near-complete loss of SA (Fig. 3c). Notably, *bbh* accumulated benzylbenzoate (Fig. 3d) and the SA loss in *bbh* could not be rescued by BA or benzylbenzoate treatment (Fig. 3e), providing supporting evidence that OsBBH functions downstream of benzylbenzoate.

Having established benzylbenzoate as an essential intermediate upstream of OsBBH, we hypothesized that benzylbenzoate—and not BA—may be the direct hydroxylation substrate of OsBBH. To test this, we transiently expressed *OsBBH* in *N. benthamiana* leaves and submerged detached leaves in benzylbenzoate solution. Control leaves expressing *mVenus* showed minimal conversion of benzylbenzoate to benzylsalicylate (Fig. 3f,g), consistent with the low expression level of the native *N. benthamiana* BBH (Extended Data Fig. 6d). By contrast, *OsBBH*-expressing leaves showed a drastic 27.9-fold increase of benzylsalicylate (Fig. 3f,g), strongly indicating that OsBBH has high hydroxylation activity toward benzylbenzoate to generate benzylsalicylate. Similarly, the *N. benthamiana* orthologues NbBBH1 and NbBBH2 showed significant BBH activity in this system (Extended Data Fig. 6e,f).

We further validated the enzymatic function of OsBBH through an *in vitro* NADPH-dependent CYP monooxygenase assay, using endoplasmic reticulum membrane-derived microsomes prepared from *OsBBH*-expressing or control *N. benthamiana* leaves. OsBBH-containing microsomes exhibited a 29.6-fold higher benzylbenzoate hydroxylation activity than the control microsomes (Extended Data Fig. 6g,h), supporting our conclusion that OsBBH has efficient hydroxylation activity toward benzylbenzoate to generate benzylsalicylate.

Further *in planta* metabolite analysis revealed nearly undetectable levels of benzylsalicylate in *bbh* leaves (Fig. 3h). Critically, exogenous benzylsalicylate restored SA levels in *bbh*, *cnl* and *bebt* (Fig. 3i,j). By contrast, benzylbenzoate restored SA levels in *cnl* and *bebt* (Extended Data Fig. 3f) but not in *bbh* (Fig. 3e).

The above results collectively resolved the search for the critical CYP hydroxylase in SA biosynthesis, demonstrating that benzylbenzoate, rather than BA, serves as the direct hydroxylation substrate for OsBBH in SA biosynthesis.

BSE catalyses the final step

The identification of benzylsalicylate as a critical intermediate suggested that a single esterase-mediated hydrolysis step could, in theory, complete SA biosynthesis by converting benzylsalicylate to SA and benzyl alcohol. Using *OsCNL1* co-expression analysis, we identified *Os05g0410200* as the most strongly co-expressed gene encoding a putative esterase or hydrolase (Fig. 4a). *Os05g0410200*, subsequently renamed benzylsalicylate esterase (OsBSE), is a member of the carboxylesterase (CXE) family⁴² and has no obvious subcellular targeting signal peptides (Extended Data Fig. 7a). Confocal imaging (Fig. 4b and Extended Data Fig. 7b), immunoblot analyses of YFP–OsBSE (Extended Data Fig. 7c) and detection of endogenous OsBSE activity (Extended Data Fig. 7d,e) collectively established the cytosolic localization of OsBSE.

To explore the biochemical activity and biological function of OsBSE, we performed a phylogenetic analysis using protein sequences of CXE family members in rice and tobacco, as well as sequences identified by BLAST searches for proteins with high sequence similarities to OsBSE and reported esterase functions. This analysis placed OsBSE in the same small subfamily alongside the tobacco NtHSR203J protein (Extended Data Fig. 4b), which was reported to have *in vitro* carboxylesterase

activity against *p*-nitrophenylbutyrate, a general substrate for esterases⁴³. Although its natural substrate and functional mechanism are unknown, silencing of NtHSR203J severely impairs pathogen-induced SA production in tobacco³⁷.

To determine whether OsBSE has benzylsalicylate esterase activity, we expressed His-tagged OsBSE in *E. coli* and tested the recombinant proteins for esterase activity using different salicylate or benzoate esters. OsBSE exhibited strong activity toward benzylsalicylate but no detectable activity toward the structurally related benzylbenzoate and cinnamylbenzoate (Fig. 4c and Extended Data Fig. 7f). We then obtained two frameshift mutants, *bse-1* and *bse-2* (Extended Data Fig. 7g), both of which exhibited near-complete elimination of SA (Fig. 4d). Metabolite analysis revealed significant accumulation of benzylsalicylate and benzylbenzoate in the *bse* mutant (Fig. 4e,f), consistent with benzylsalicylate being the substrate for OsBSE and benzylbenzoate being an upstream intermediate. Together, our data support the role of OsBSE in the final step of SA biosynthesis by catalysing the conversion of benzylsalicylate to SA.

Further validation of BSE and BBH

To further verify the *in vivo* catalytic action of OsBBH and OsBSE, we conducted stable isotope-labelled substrate feeding experiments using rice *bebt*, *bbh* and *bse* mutants. When fed with deuterium-labelled benzylbenzoate, *bebt* mutants produced deuterium-labelled SA at levels similar to those in wild-type plants (Fig. 4g). This finding aligns with our model proposing that benzylbenzoate is the product of OsBEBT that can complement the SA-deficient phenotype of the *bebt* mutant (Extended Data Fig. 3f). By contrast, *bbh* and *bse* mutants had almost no detectable deuterium-labelled SA (Fig. 4g), confirming benzylbenzoate as an upstream precursor for both OsBBH and OsBSE. Moreover, deuterium-labelled benzylsalicylate accumulated in the *bse* mutant but remained undetectable in the *bbh* mutant (Fig. 4g), consistent with the notion that OsBBH hydroxylates benzylbenzoate and OsBSE hydrolyses benzylsalicylate.

The sequential biochemical functions of OsBBH and OsBSE were additionally validated in *N. benthamiana* leaves transiently expressing *OsBBH* alone or in combination with *OsBSE*, followed by benzylbenzoate supplementation. Whereas control leaves treated with benzylbenzoate alone showed low levels of SA and benzylsalicylate, expression of *OsBBH* resulted in substantial accumulation of benzylsalicylate owing to OsBBH-catalysed benzylbenzoate hydroxylation, accompanied by only a modest increase in SA levels (Fig. 4h). Furthermore, co-expression of *OsBBH* and *OsBSE* led to massive depletion of benzylsalicylate and a marked increase in SA levels, supporting a role for OsBSE in benzylsalicylate hydrolysis (Fig. 4h). Consistently, expression of OsBSE alone decreased benzylsalicylate to undetectable levels and modestly increased SA compared with the control (Fig. 4h).

In summary, our complementary *in vivo* isotope labelling and enzyme reconstitution experiments established the sequential action of BBH and BSE in converting benzylbenzoate to SA through the benzylsalicylate intermediate (Fig. 5a).

Conservation of the BEBT–BBH–BSE module

Previous studies using isotope labelling, chemical inhibition and gene silencing (Extended Data Fig. 2a–c), as well as gene disruption^{5,17,23,28,38,40}, together support the conserved importance of the phenylalanine-derived route of SA biosynthesis. To this end, we tested whether the OsBEBT–OsBBH–OsBSE biosynthetic module (Fig. 5a) has an important role in pathogen response and in plant species beyond rice.

Consistent with our recent report that OsCNL is important for resistance to rice blast (*Magnaporthe oryzae*)⁵, *bebt*, *bbh* and *bse* exhibited

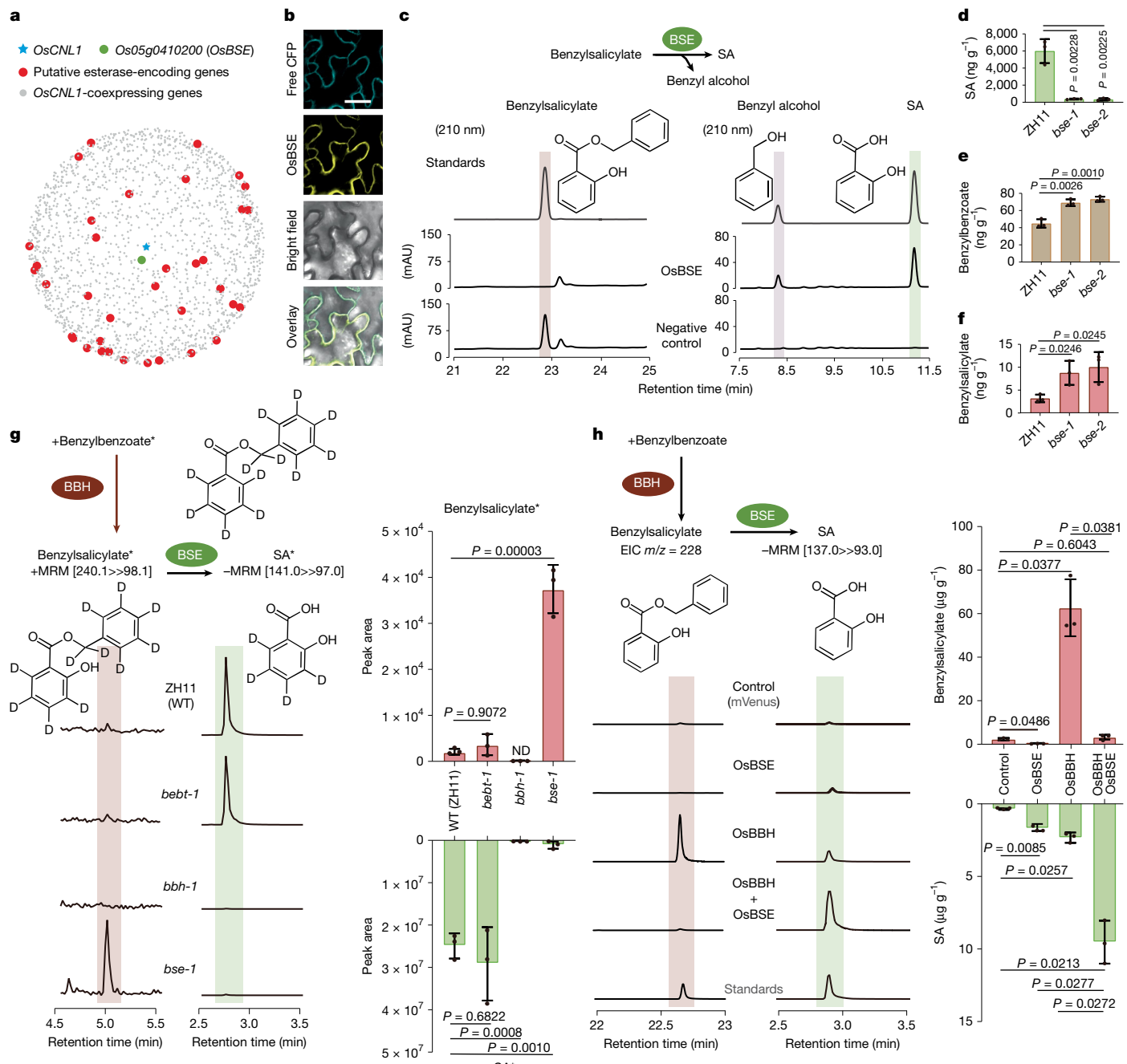


Fig. 4 | OsBSE hydrolyses benzylsalicylate to release SA. **a**, Gene co-expression network analysis identifying putative esterase-encoding genes co-expressed with OsCNL1. **b**, Confocal microscopy images show co-localization of YFP–OsBSE and cytosolic CFP in *N. benthamiana* leaf epidermis. Scale bar, 30 μ m. **c**, In vitro enzymatic activity analysis of OsBSE. HPLC chromatograms (absorbance at 210 nm) show substrate consumption and product formation when purified recombinant OsBSE was incubated with benzylsalicylate. Heat-inactivated enzyme served as the control. **d–f**, Metabolite analysis of leaves from two-week-old wild-type ZH11 and *bse* rice. SA (**d**), benzylbenzoate (**e**) and benzylsalicylate (**f**) were quantified by LC–MS/MS with MRM and normalized to fresh weight. Data are mean \pm s.d. ($n = 3$ biologically independent samples). Statistical significance was determined by two-tailed Student's *t*-tests. **g**, Metabolic tracking using deuterium-labelled BA in five-day-old rice leaves. Metabolites from equal-weight leaf tissue were analysed by LC–MS/MS with MRM. Left, representative LC–MS chromatograms of deuterium-labelled

metabolites. Peak intensities are shown relative to the highest signal for each compound. Right, peak area quantification for labelled benzylsalicylate and SA. Data are mean \pm s.d. ($n = 3$ biologically independent samples). Statistical significance was determined by one-way ANOVA with post hoc Tukey HSD test. **h**, Reconstitution of the final two steps of SA biosynthesis in *N. benthamiana*. Leaves transiently expressing OsBBH, OsBSE, their combination or mVenus (control) were fed with benzylbenzoate, followed by metabolite extraction. Benzylsalicylate was analysed by GC–MS (EIC, $m/z = 228$) and SA by LC–MS/MS with MRM. Metabolite levels were normalized to fresh weight. Data are mean \pm s.d. ($n = 3$ independent experiments). Statistical significance was determined by Welch's ANOVA followed by Games–Howell post hoc tests. Asterisks indicate deuterium-labelled metabolites; + and – denote positive and negative ionization modes, respectively. MRM transition parameters are indicated above chromatograms.

Article

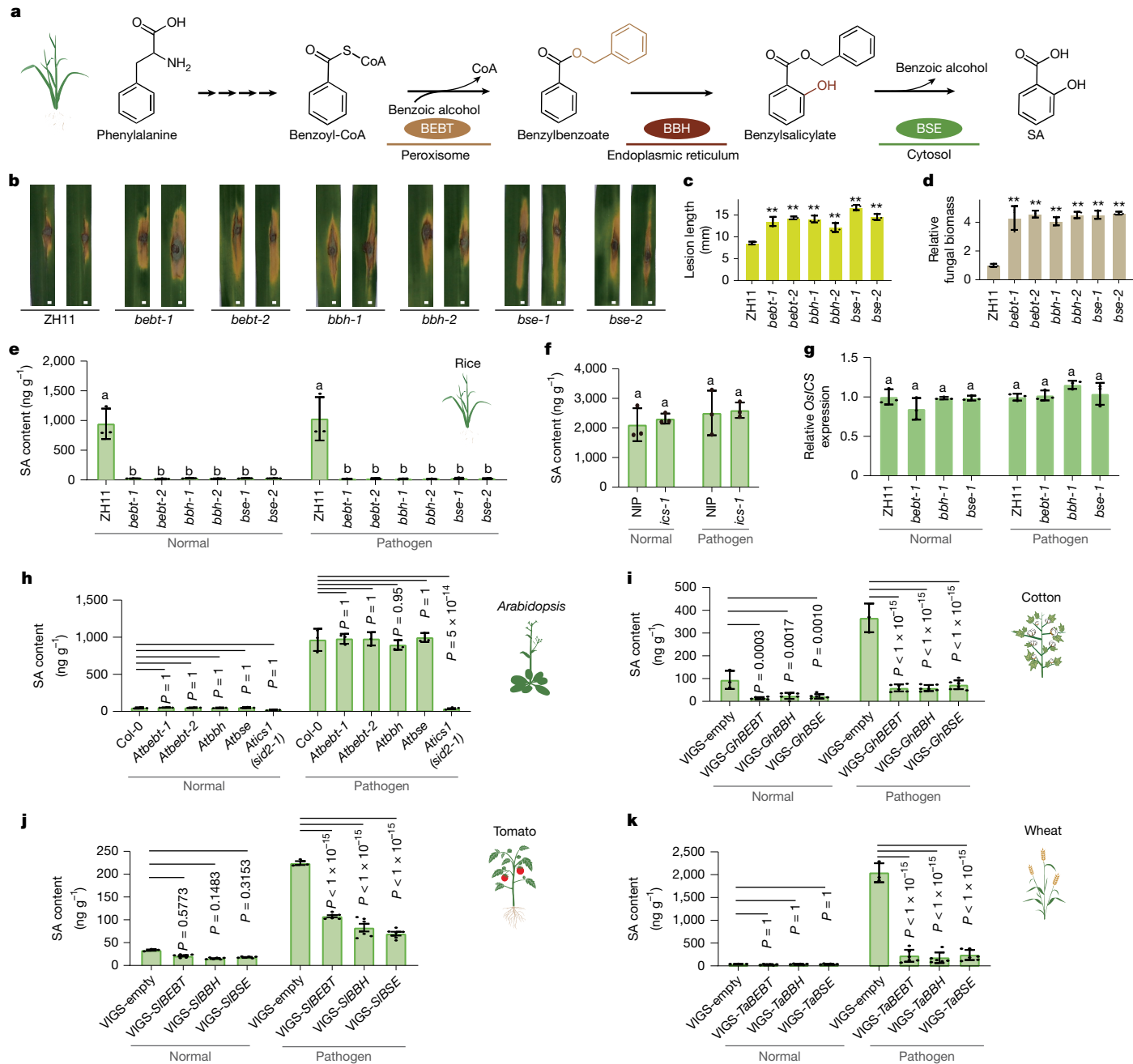


Fig. 5 | The BEBT-BBH-BSE module is conserved in plant SA biosynthesis. **a**, Working model of phenylalanine-derived SA biosynthesis in rice, highlighting the sequential action of BEBT, BBH and BSE enzymes. **b–d**, Disease resistance analysis of rice mutants following *M. oryzae* (strain RB2) infection. Shown are representative images of disease lesions. Scale bars, 1 mm (**b**), quantification of lesion length using ImageJ (**c**) and pathogen growth assessment using DNA-based quantitative PCR (qPCR) by calculating the threshold cycle value of *MoPot2* relative to the rice ubiquitin gene (*OsUBIQUITIN*) (**d**). Data are mean \pm s.d. ($n = 3$ biologically independent samples). In **c,d**, statistical significance was determined by two-tailed Student's *t*-tests. ** $P < 0.01$. **e,f**, SA accumulation in 14-day-old rice mutants. Data are mean \pm s.d. ($n = 3$ biologically independent samples). **g**, *OsCS* expression analysis in 14-day-old rice mutants using qPCR with reverse transcription (RT-qPCR). Data are mean \pm s.d. ($n = 3$ biologically independent samples).

($n = 3$ biologically independent samples). **h**, SA quantification in 30-day-old *Arabidopsis* mutants with or without *Pseudomonas syringae* DC3000 infection. Data are mean \pm s.d. ($n = 3$ biologically independent samples). **i–k**, SA levels in VIGS-silenced plants following pathogen infection. Plants were individually silenced for BEBT, BBH or BSE homologues using VIGS. SA was quantified in cotton infected with *Verticillium dahliae* V991 (**i**), tomato infected with *P. syringae* DC3000 (**j**) and wheat infected with *Fusarium graminearum* (**k**). Data are mean \pm s.d. (control: $n = 3$ biologically independent samples; VIGS-treated: $n = 6$ biologically independent samples). In **e,f,h–k**, SA content was analysed by LC-MS/MS with MRM and normalized to fresh weight. In **e–g,h–k**, statistical significance was determined by one-way ANOVA with post hoc Tukey HSD test. In **e–g**, different letters indicate significant differences ($P < 0.05$).

significantly compromised resistance to this pathogen (Fig. 5b–d). Furthermore, the contents of leaf SA and its derivative SA glycoside (SAG) were almost undetectable in *bebt*, *bbh* and *bse*, with or without *M. oryzae* infection (Fig. 5e and Extended Data Fig. 8a). Consistent

with a previous study⁴⁴, wild-type rice does not show obvious pathogen-induced accumulation of SA and SAG (Fig. 5e and Extended Data Fig. 8a), probably owing to the already extremely high basal concentration of SA. Notably, knockout of the rice homologue of *AtICS* had

no effect on SA accumulation under normal or pathogen-challenged conditions (Fig. 5f), and *OsICS* expression remained unchanged in pathogen-challenged *bebt*, *bbh* and *bse* mutants (Fig. 5g). These data further support our conclusion that the BEBT–BBH–BSE module, rather than the ICS pathway, is mainly responsible for SA biosynthesis and pathogen resistance in rice.

We then explored whether the role of the BEBT–BBH–BSE module is conserved beyond rice. In tobacco, silencing of the OsBEBT homologue NtHSR201 or the OsBSE homologue NtHSR203J severely impairs pathogen-induced SA production³⁷. The inhibition of SA biosynthesis by CYP inhibitors across plant species (Extended Data Fig. 2b) also suggests the functional conservation of OsBBH-mediated hydroxylation. To assess this conservation, we investigated the role of the BEBT–BBH–BSE module in SA production in *Arabidopsis* (Brassicaceae) and three economically important crops: wheat (*T. aestivum*, Gramineae), cotton (*Gossypium hirsutum*, Malvaceae) and tomato (*Solanum lycopersicum*, Solanaceae), all of which showed apparent pathogen-induced SA accumulation (Fig. 5h–k). On the basis of reciprocal protein BLAST, we identified putative orthologues for *BEBT*, *BBH* and *BSE* in these plants. For functional analysis, we obtained *Arabidopsis* transfer DNA (T-DNA) insertion mutants, and used virus-induced gene silencing (VIGS) in wheat, cotton and tomato, resulting in successful inhibition of gene expression in all cases (Extended Data Fig. 9a,b). In *Arabidopsis*, disruption of these genes did not affect the levels of SA (Fig. 5h) or its derivatives SAG and SA glucose ester (SGE) (Extended Data Fig. 8b) or the transcription of *PATHOGENESIS-RELATED 1* (*PRI*) (Extended Data Fig. 9c), a widely used marker gene for SA-dependent defence responses, under either normal or pathogen-infected conditions. This is in sharp contrast to the severe reduction of SA, SAG, SGE and *PRI* transcription in the *Arabidopsis* ICS mutant *sid2-1* (Fig. 5h and Extended Data Figs. 8b and 9c), confirming that *Arabidopsis* primarily uses the ICS pathway for SA biosynthesis. Of note, silencing any of the genes in the BEBT–BBH–BSE module severely compromised pathogen-induced SA and SAG production and *PRI* transcription in wheat, cotton and tomato (Fig. 5i–k and Extended Data Figs. 8c and 9d), demonstrating the functional conservation of this three-enzyme cascade in pathogen response across major crop families.

Analysis of public transcriptome data of 24 economically valuable plant species revealed that putative orthologous genes of *BEBT*, *BBH* and *BSE* are generally pathogen-inducible in diverse plant species (Extended Data Fig. 10). However, in the two Brassicaceae species *Arabidopsis* and *Brassica napus*, these three genes appear to be less or not at all pathogen-inducible, and expression of key genes of the ICS pathway shows limited pathogen response in species outside of Brassicaceae (Extended Data Fig. 10), a pattern that was also previously noted for ICS in poplar and tobacco^{45,46}. These observations indicate that the BEBT–BBH–BSE module may have critical roles in SA biosynthesis and immune response in many important crops.

Discussion

Our identification of the BEBT–BBH–BSE module advances our understanding of phenylalanine-derived SA biosynthesis. For decades, BA was believed to be a direct precursor of SA through CYP-mediated hydroxylation^{1,47}, but our findings in rice conclusively refute this model. Supporting this, *bebt*, *bbh* and *bse* rice mutants display strong accumulation of BA (Fig. 2a and Extended Data Fig. 7h,i) and a nearly complete loss of SA (Figs. 1f, 3c and 4d). Furthermore, we identified OsBBH as the CYP in this pathway, establishing benzylbenzoate, rather than BA, as the authentic substrate of OsBBH.

Converting benzyl-CoA (871 Da) into benzylbenzoate (212 Da), a much smaller molecule, may facilitate the export of the benzyl moiety out of the peroxisomal membrane. The export of benzylbenzoate may involve active transporters, such as ATP-binding

cassette (ABC) transporters, or non-selective channels (for small molecules below 300–400 Da), such as 22-kDa peroxisomal membrane protein (PMP22)^{22,48}. Considering the hydrophobic property of benzylbenzoate, membrane contact sites between peroxisomes and the endoplasmic reticulum might also facilitate its transport. In previous studies, the transfer of hydrophobic substances, such as cholesterol transfer by oxysterol-binding protein (OSBP) or ceramide transfer by ceramide transfer protein (CERT), often relies on membrane contact sites⁴⁹. Moreover, owing to the limitation of our current understanding on endoplasmic reticulum transport mechanisms, it is difficult to speculate on the mechanisms that guide endoplasmic reticulum transport of benzylbenzoate or benzylsalicylate. However, given that benzylsalicylate is less hydrophobic than benzylbenzoate, we cannot exclude the possibility that this occurs through diffusion.

The fact that exogenous BA can increase SA levels (Fig. 2b) and isotope-labelled BA can be incorporated into benzyl-CoA, benzylbenzoate and SA (Fig. 2c–f) suggests that when the cytosolic BA level reaches a threshold, some may be imported into peroxisomes and converted into benzyl-CoA, which is then utilized by OsBEBT. However, given the nearly complete elimination of SA in *cnl* leaves (Fig. 1f), benzyl-CoA directly from the peroxisomal cinnamyl-CoA β-oxidation is likely to be the major SA precursor in rice leaves. Further, feeding isotope-labelled BA to wild-type rice caused both benzene rings on benzylbenzoate to be labelled (Fig. 2f), indicating that exogenously added BA is not only activated to benzyl-CoA but also reduced to benzyl alcohol. This finding is not surprising considering that BA can be reduced to benzyl alcohol in planta⁵⁰ and the exogenously added BA is most probably in excess. The biological significance of this observation may be worth investigating in future studies.

Our transient assays in *N. benthamiana* leaves support the catalytic order of the BEBT–BBH–BSE cascade in SA production. When benzylbenzoate was exogenously added to the control *N. benthamiana* leaves, benzylsalicylate and SA were still at relatively low levels (Figs. 3g and 4h). Transient expression of *OsBBH* or *NbBBH* strongly increases benzylsalicylate levels (Figs. 3g and 4h and Extended Data Fig. 6f), whereas SA is only mildly increased (Fig. 4h). Additional expression of *OsBSE* strongly increases SA and decreases benzylsalicylate (Fig. 4h). Furthermore, without exogenous precursor supplementation, over-expressing *OsCNL* alone causes a significant increase in SA levels (Extended Data Fig. 7j). When expressed alongside *OsCNL*, only *OsBEBT*—but not *OsBBH* or *OsBSE*—further enhances SA accumulation (Extended Data Fig. 7k), consistent with the proposed order of the cascade. One intriguing open question is the cause of the extremely high basal levels of SA and the apparent imbalance between SA content and its upstream intermediate in rice. The mechanistic basis for this phenomenon requires further investigation.

Although the ICS pathway does not appear to be important for SA biosynthesis in rice leaves under normal and pathogen-infected conditions (Fig. 5f), it may be active in other tissues or stress conditions. The two SA biosynthetic pathways may co-exist in various plant species and organs and respond differentially to different environmental conditions, together ensuring robust SA production under diverse physiological settings.

Although simply changing SA levels may not be a universally viable strategy for engineering disease-resistant crops, our work has significant implications in crop immunity research. The BEBT–BBH–BSE module is important for rice disease resistance (Fig. 5b–d) and transcriptionally responsive to pathogens in many crops (Extended Data Fig. 9b). Our genetic studies in wheat, cotton and tomato supported the requirement for this module in pathogen-induced SA biosynthesis in these important crops (Fig. 5i–k). Finally, unlike the rice mutants of *PAL*²⁵, *AIM1*²³ or *ICS*¹⁸, there are no obvious growth defects in *bebt*, *bbh* or *bse* mutants (Extended Data Fig. 8d), supporting the functional specificity of these newly-identified enzymes. Taken together, the

conservation of the BEBT–BBH–BSE module, as well as its specificity in SA biosynthesis, underscores its broad potential to guide breeding efforts for crop disease resistance.

Online content

Any methods, additional references, Nature Portfolio reporting summaries, source data, extended data, supplementary information, acknowledgements, peer review information; details of author contributions and competing interests; and statements of data and code availability are available at <https://doi.org/10.1038/s41586-025-09280-9>.

1. Ullah, C., Chen, Y.-H., Ortega, M. A. & Tsai, C.-J. The diversity of salicylic acid biosynthesis and defense signaling in plants: knowledge gaps and future opportunities. *Curr. Opin. Plant Biol.* **72**, 102349 (2023).
2. Spoel, S. H. & Dong, X. Salicylic acid in plant immunity and beyond. *Plant Cell* **36**, 1451–1464 (2024).
3. Desborough, M. J. R. & Keeling, D. M. The aspirin story—from willow to wonder drug. *Br. J. Haematol.* **177**, 674–683 (2017).
4. Zou, Z. et al. Biochemical pathways of salicylic acid derived from L-phenylalanine in plants with different basal SA levels. *J. Agric. Food Chem.* **72**, 2898–2910 (2024).
5. Wang, Y. et al. Species- and organ-specific contribution of peroxisomal cinnamate:CoA ligases to benzoic and salicylic acid biosynthesis. *Plant Cell* **37**, koae329 (2025).
6. Rivas-San Vicente, M. & Plasencia, J. Salicylic acid beyond defence: its role in plant growth and development. *J. Exp. Bot.* **62**, 3321–3338 (2011).
7. Lebeis, S. L. et al. Salicylic acid modulates colonization of the root microbiome by specific bacterial taxa. *Science* **349**, 860–864 (2015).
8. Mohamed, H. I., El-Shazly, H. H. & Badr, A. In *Plant Phenolics in Sustainable Agriculture* (eds Lone, R., Shuhab, R. & Kamili, A. N.) 533–554 (Springer, 2020).
9. Wildermuth, M. C., Dewdney, J., Wu, G. & Ausubel, F. M. Isochorismate synthase is required to synthesize salicylic acid for plant defence. *Nature* **414**, 562–565 (2001).
10. Rekhter, D. et al. Isochorismate-derived biosynthesis of the plant stress hormone salicylic acid. *Science* **365**, 498–502 (2019).
11. Torrens-Spence, M. P. et al. PBS3 and EPS1 complete salicylic acid biosynthesis from isochorismate in *Arabidopsis*. *Mol. Plant* **12**, 1577–1586 (2019).
12. Hao, Q. et al. Isochorismate-based salicylic acid biosynthesis confers basal resistance to *Fusarium graminearum* in barley. *Mol. Plant Pathol.* **19**, 1995–2010 (2018).
13. Zhang, Y.-Z. et al. Investigating the mechanisms of isochorismate synthase: An approach to improve salicylic acid synthesis and increase resistance to *Fusarium* head blight in wheat. *Crop J.* **12**, 1054–1063 (2024).
14. Shine, M. B. et al. Cooperative functioning between phenylalanine ammonia lyase and isochorismate synthase activities contributes to salicylic acid biosynthesis in soybean. *New Phytol.* **212**, 627–636 (2016).
15. Zhang, H. et al. PAL-mediated SA biosynthesis pathway contributes to nematode resistance in wheat. *Plant J.* **107**, 698–712 (2021).
16. Qin, Y. et al. Barley isochorismate synthase mutant is phylloquinone-deficient, but has normal basal salicylic acid level. *Plant Signal Behav.* **14**, 1671122 (2019).
17. Jia, X. et al. The origin and evolution of salicylic acid signaling and biosynthesis in plants. *Mol. Plant* **16**, 245–259 (2023).
18. Wang, Z. et al. Isochorismate synthase is required for phylloquinone, but not salicylic acid biosynthesis in rice. *aBIO/TECH* **5**, 488–496 (2024).
19. Garcion, C. et al. Characterization and biological function of the ISOCHORISMATE SYNTHASE gene of *Arabidopsis*. *Plant Physiol.* **147**, 1279–1287 (2008).
20. Zhang, X. & Liu, C.-J. Multifaceted regulations of gateway enzyme phenylalanine ammonia-lyase in the biosynthesis of phenylpropanoids. *Mol. Plant* **8**, 17–27 (2015).
21. Widhalm, J. R. & Dudareva, N. A familiar ring to it: biosynthesis of plant benzoic acids. *Mol. Plant* **8**, 83–97 (2015).
22. Pan, R., Liu, J., Wang, S. & Hu, J. Peroxisomes: versatile organelles with diverse roles in plants. *New Phytol.* **225**, 1410–1427 (2020).
23. Xu, L. et al. ABNORMAL INFLORESCENCE MERISTEM1 functions in salicylic acid biosynthesis to maintain proper reactive oxygen species levels for root meristem activity in rice. *Plant Cell* **29**, 560–574 (2017).
24. Pan, R., Liu, J. & Hu, J. Peroxisomes in plant reproduction and seed-related development. *J. Integr. Plant Biol.* **61**, 784–802 (2019).
25. He, J. et al. An R2R3 MYB transcription factor confers brown planthopper resistance by regulating the phenylalanine ammonia-lyase pathway in rice. *Proc. Natl Acad. Sci. USA* **117**, 271–277 (2020).
26. Leon, J., Yalpani, N., Raskin, I. & Lawton, M. A. Induction of benzoic acid 2-hydroxylase in virus-inoculated tobacco. *Plant Physiol.* **103**, 323–328 (1993).
27. León, J., Shulaev, V., Yalpani, N., Lawton, M. A. & Raskin, I. Benzoic acid 2-hydroxylase, a soluble oxygenase from tobacco, catalyzes salicylic acid biosynthesis. *Proc. Natl Acad. Sci. USA* **92**, 10413–10417 (1995).
28. Wang, Y. et al. A peroxisomal cinnamate:CoA ligase-dependent phytohormone metabolic cascade in submerged rice germination. *Dev. Cell* **59**, 1363–1378.e4 (2024).
29. Lackus, N. D., Schmidt, A., Gershenson, J. & Källner, T. G. A peroxisomal β-oxidative pathway contributes to the formation of C₆–C₁ aromatic volatiles in poplar. *Plant Physiol.* **186**, 891–909 (2021).
30. Klempien, A. et al. Contribution of CoA ligases to benzenoid biosynthesis in *Petunia* flowers. *Plant Cell* **24**, 2015–2030 (2012).
31. Jung, K. H. et al. Development of defense signaling pathways against bacterial blight disease in rice using genome-wide transcriptome data. *J. Agric. Sci.* **6**, p48 (2014).
32. Deng, Q. et al. Comprehensive identification of plant peroxisome targeting signal type 1 tripeptides. *New Phytol.* **243**, 1642–1650 (2024).
33. Kumar, G. et al. Characterization of evolutionarily distinct rice BAHD-Acyltransferases provides insight into their plausible role in rice susceptibility to *Rhizoctonia solani*. *Plant Genome* **14**, e20140 (2021).
34. D'Auria, J. C., Chen, F. & Pichersky, E. Characterization of an acyltransferase capable of synthesizing benzylbenzoate and other volatile esters in flowers and damaged leaves of *Clarkia breweri*. *Plant Physiol.* **130**, 466–476 (2002).
35. Boatright, J. et al. Understanding in vivo benzenoid metabolism in *Petunia* petal tissue. *Plant Physiol.* **135**, 1993–2011 (2004).
36. Chedgy, R. J., Källner, T. G. & Constabel, C. P. Functional characterization of two acyltransferases from *Populus trichocarpa* capable of synthesizing benzyl benzoate and salicyl benzoate, potential intermediates in salicinoid phenolic glycoside biosynthesis. *Phytochemistry* **113**, 149–159 (2015).
37. Takagi, K., Tasaki, K., Komori, H. & Katou, S. Hypersensitivity-related genes *HSR201* and *HSR203J* are regulated by calmodulin-binding protein 60-type transcription factors and required for pathogen signal-induced salicylic acid synthesis. *Plant Cell Physiol.* **63**, 1008–1022 (2022).
38. Kotera, Y. et al. The peroxisomal β-oxidative pathway and benzyl alcohol O-benzoyltransferase HSR201 cooperatively contribute to the biosynthesis of salicylic acid. *Plant Cell Physiol.* **64**, 758–770 (2023).
39. Kotera, Y. et al. Peroxisomal localization of benzyl alcohol O-benzoyltransferase HSR201 is mediated by a non-canonical peroxisomal targeting signal and required for salicylic acid biosynthesis. *Plant Cell Physiol.* **65**, 2054–2065 (2024).
40. Xu, L. et al. AIM1-dependent high basal salicylic acid accumulation modulates stomatal aperture in rice. *New Phytol.* **238**, 1420–1430 (2023).
41. Adebesin, F., Widhalm, J. R., Lynch, J. H., McCoy, R. M. & Dudareva, N. A peroxisomal thioesterase plays auxiliary roles in plant β-oxidative benzoic acid metabolism. *Plant J.* **93**, 905–916 (2018).
42. Cummins, I., Landrum, M., Steel, P. G. & Edwards, R. Structure activity studies with xenobiotic substrates using carboxylesterases isolated from *Arabidopsis thaliana*. *Phytochemistry* **68**, 811–818 (2007).
43. Pontier, D. et al. In *Bacterial Wilt Disease: Molecular and Ecological Aspects* (eds Prior, P., Allen, C. & Elphinstone, J.) 203–208 (Springer, 1998).
44. Silverman, P. et al. Salicylic acid in rice (biosynthesis, conjugation, and possible role). *Plant Physiol.* **108**, 633–639 (1995).
45. Yuan, Y. et al. Alternative splicing and gene duplication differentially shaped the regulation of isochorismate synthase in *Populus* and *Arabidopsis*. *Proc. Natl Acad. Sci. USA* **106**, 22020–22025 (2009).
46. Ogawa, D. et al. The phenylalanine pathway is the main route of salicylic acid biosynthesis in Tobacco mosaic virus-infected tobacco leaves. *Plant Biotechnol.* **23**, 395–398 (2006).
47. Lefevere, H., Bauters, L. & Gheysen, G. Salicylic acid biosynthesis in plants. *Front. Plant Sci.* **11**, 338 (2020).
48. Charton, L., Plett, A. & Linka, N. Plant peroxisomal solute transporter proteins. *J. Integr. Plant Biol.* **61**, 817–835 (2019).
49. Jain, A. & Zoncu, R. Organelle transporters and inter-organelle communication as drivers of metabolic regulation and cellular homeostasis. *Mol. Metab.* **60**, 101481 (2022).
50. Babst, B. A., Harding, S. A. & Tsai, C. J. Biosynthesis of phenolic glycosides from phenylpropanoid and benzenoid precursors in *Populus*. *J. Chem. Ecol.* **36**, 286–297 (2010).

Publisher's note Springer Nature remains neutral with regard to jurisdictional claims in published maps and institutional affiliations.



Open Access This article is licensed under a Creative Commons Attribution-NonCommercial-NoDerivatives 4.0 International License, which permits any non-commercial use, sharing, distribution and reproduction in any medium or format, as long as you give appropriate credit to the original author(s) and the source, provide a link to the Creative Commons licence, and indicate if you modified the licensed material. You do not have permission under this licence to share adapted material derived from this article or parts of it. The images or other third party material in this article are included in the article's Creative Commons licence, unless indicated otherwise in a credit line to the material. If material is not included in the article's Creative Commons licence and your intended use is not permitted by statutory regulation or exceeds the permitted use, you will need to obtain permission directly from the copyright holder. To view a copy of this licence, visit <http://creativecommons.org/licenses/by-nc-nd/4.0/>.

© The Author(s) 2025

Methods

Chemicals and reagents

The following chemical reagents were procured from commercial suppliers: BA, benzylbenzoate, benzylsalicylate and phenethyl phenylacetate from Shanghai Macklin Biochemical Technology. SGE (ZB-240319) from Shanghai ZZBIO; and deuterium-labelled BA (HY-N0216S) and benzylbenzoate (HY-B0935S1) were purchased from MedChemExpress. SAG was provided by C. Song.

For molecular and biochemical assays, the following kits were used: RNA extraction kit (Easy-Do, DR0409050), reverse transcription kit (TransGen Biotech, AE311-02), qPCR kit (Vazyme Biotech, Q711-02), Clonexpress II One Step Cloning Kit (Vazyme Biotech, C11202). Enzyme activity assays were performed using Alcohol Dehydrogenase Activity Assay Kit (Beyotime Biotechnology, S0241S), Catalase (CAT) Assay Kit (Beijing Solarbio Science and Technology, BC0200), Protein Marker (Yeasen Biotechnology, 26616ES72), and the Bradford Protein Assay Kit (Coolaber, SK1060). For cloning and protein expression, the following competent cells were used: DH5 α (Tsingke, TSC-C01), Rosetta 2 Competent cells (Weidi, EC1014) and GV3101 (Angyubio G6039).

Plant materials and growth conditions

The rice (*O. sativa*) mutants *cnl*, *bebt*, *bbh* and *bse* are on the background of the japonica cultivar ZH11 (zhonghua11), and the rice mutants *te1*, *te2* and *ics1* are on the background of the japonica cultivar NIP (Nipponbare). The *cnl* mutants were generated in our previous study²⁸, and *bebt*, *bbh* and *bse* mutants are CRISPR–Cas9 mutants obtained from Biogle Genetech (<https://www.biogle.cn>). The rice *te1 te2* mutants were generated using CRISPR–Cas9 and *ics1* mutants were obtained from J.-L. Qiu¹⁸. Rice seeds were collected at maturity and dried at 42 °C for 4 days to break seed dormancy and fully filled seeds were selected for experiments. In the greenhouse, except for the rice plants used for pathogen treatment experiments, all rice plants were grown under a 14 h:10 h light:dark photoperiod, 30 °C/28 °C day/night temperature, and 85% humidity. Rice plants used for pathogen treatment experiments were grown in trays filled with field soil under the 14:h light:10 h dark photoperiod, 28 °C/26 °C day/night temperature, and 60% humidity. The *Arabidopsis thaliana* mutants *Atbebt-1* (SALK_030095), *Atbebt-2* (SALK_089260), *Atbse* (SALK_205911) and *Atbbh* (SALK_039417), obtained from *Arabidopsis* Biological Resource Center (ABRC), were grown in a growth chamber under 16 h:8 h light:dark and 22 °C/20 °C day/night cycles. *Atics1* (*sid2-1*) was reported in a previous study⁹. The tomato (*S. lycopersicum* L. cultivar M82) seedlings were grown in a growth chamber under 16 h:8 h light:dark photoperiod, 24 °C/22 °C day/night temperature, and 60% humidity. The wheat (*T. aestivum* L.) seedlings were grown in a growth chamber under 16 h:8 h light:dark photoperiod, 23 °C/21 °C day/night temperature, and 60% humidity. The cotton (*G. hirsutum* L. cultivar TM-1) seedlings were grown in a growth chamber under a 16 h:8 h, light:dark photoperiod, 25 °C/23 °C day/night temperature, and 40% humidity. *N. benthamiana* plants were grown in a growth chamber at 22 °C with 16-h:8-h light:dark photoperiod, 22 °C/20 °C day/night temperature, and 60% humidity.

RNA extraction and vector construction

Total RNA was extracted using the Rice RNA Rapid Extraction Kit (Easy-Do, DR0409050) and was reverse-transcribed using the reverse transcription kit (TransGen Biotech, AE311-02), after which cDNA was used for gene cloning and RT–qPCR. qPCR was performed according to instructions from the qPCR kit (Vazyme Biotech, Q713-02) using the Light Cycler Instrument 480 II (Roche). Vectors were constructed by homologous recombination using Clonexpress II One Step Cloning Kit (Vazyme Biotech, C11202). Primers for gene cloning are listed in Supplementary Table 1, RT–qPCR, semi-quantitative PCR, DNA-based qPCR, rice mutant characterization, and restriction enzyme sites and

plasmids used for subcellular localization, transient expression, recombinant protein expression and VIGS are listed in Supplementary Table 2.

Transient protein expression in plant cells

Vectors used for Agrobacterium-mediated transient expression in *N. benthamiana* were transformed into *A. tumefaciens* strain GV3101, using the freeze-thaw method, and spread onto LB agar plates (50 µg ml⁻¹ kanamycin and 30 µg ml⁻¹ rifampicin) to grow at 28 °C for 2 days. The positive transformants were inoculated into 2 ml of liquid LB cultures (50 µg ml⁻¹ kanamycin and 30 µg ml⁻¹ rifampicin) with shaking for 16 h at 30 °C. GV3101 were collected by centrifugation at 6,000g for 5 min and resuspended in 10 mM MgCl₂ solution containing 200 µM acetosyringone and later injected into the abaxial surface of 4- to 6-week-old *N. benthamiana* leaves with a needleless syringe, after which the infiltrated leaves were collected for analysis within 2–3 days⁵¹. For protoplast transformation, polyethylene glycol-mediated transfection of isolated rice protoplasts were performed as described previously⁵².

Subcellular localization

To determine protein subcellular localization, infiltrated *N. benthamiana* leaves were collected 48 h post-infiltration for observation, and the transformed rice protoplasts were incubated in darkness for 12–16 h before observation. The endoplasmic reticulum marker ER-rk, which was created by fusing the signal peptide of AtWAK2 (*Arabidopsis* wall-associated kinase2) at the N-terminus of the mCherry protein and the endoplasmic reticulum retention signal His-Asp-Glu-Leu at its C-terminus, was obtained from ABRC (CD3-959). A Fluoview FV3000 confocal laser-scanning microscope (Olympus) was used for image capturing in epidermal cells, where CFP was excited with 414 nm lasers and detected at 460–500 nm, YFP was excited with 475 nm lasers and detected at 505–550 nm, and mCherry was excited with 587 nm lasers and detected at 600–650 nm.

Expression of recombinant proteins in *E. coli*

Protein expression in *E. coli* was conducted using a previously reported method²⁸. Constructs for the His-tagged recombinant proteins were first transformed into *E. coli* Rosetta (Weidi, EC1014), cultured in 1 ml LB medium overnight at 37 °C with 220 rpm of shaking, and then added to 100 ml LB medium for incubation for 2–3 h at 37 °C with 220 rpm of shaking. After the bacterial OD₆₀₀ reached 0.4–0.5, 0.5 mM isopropyl β-D-1-thiogalactopyranoside was added, and the mixture was incubated overnight at 18 °C with shaking at 120 rpm. The bacteria were subsequently collected by centrifugation and resuspended in 30 ml lysis buffer (20 mM Tris-HCl, 200 mM NaCl, 1 mM EDTA, pH 7.4), lysed by sonication followed by centrifugation at 12,000 rpm for 1 h. The supernatant was collected, from which the recombinant proteins were purified using Ni-NTA beads (Smart lifesciences, SA003025). Protein concentration was determined using the Bradford Protein Assay Kit (Coolaber, SK1060) according to the manufacturer's instructions.

Feeding of BA, benzylbenzoate and benzylsalicylate to rice seedlings

BA, benzylbenzoate, benzylsalicylate, deuterium-labelled BA and deuterium-labelled benzylbenzoate were dissolved in isopropanol to prepare a 200 mM stock solution, which was then diluted to a working concentration of 200 µM using water containing 0.01% Silwet-L77. Rice seeds were immersed in the solution and grown in a greenhouse under a 14 h:10 h light:dark photoperiod and 30 °C/28 °C day/night temperature. After five days of growth, the metabolites in the emerged leaves were extracted and analysed.

Enzymatic characterization of OsTE

The thioesterase activity of OsTE was assayed according to a previous report⁴¹, with minor modifications. In brief, 150 µl buffer containing

Article

50 mM KH₂PO₄ at pH 7.0 with the addition of 500 μM benzoyl-CoA or cinnamoyl-CoA were mixed with 1 μg of purified recombinant proteins in 10 μl solution, and incubated at 28 °C. After 60 min, the reaction was terminated by adding 80 μl 10% trichloroacetic acid aqueous solution, and was sent for analysis by HPLC.

For enzyme kinetic analysis, 1 μg recombinant protein was added to 150 μl of the assay buffer containing varied concentrations of substrate (3.9 μM to 500 μM). After 1 min at 28 °C, the reaction was terminated, and the production of BA or cinnamic acid was analysed by ultrahigh performance liquid chromatography (UHPLC).

Enzymatic characterization of OsBEBT

The acyltransferase activity of OsBEBT was assayed according to a previous report³⁶, with minor modifications. For reactions, each substrate (500 μM) was incubated with 1 μg purified recombinant protein in a total volume of 150 μl of the reaction buffer that consisted of 50 mM Tris-HCl and 300 mM NaCl (pH 7.0). After incubating at 28 °C for 60 min, the reaction was terminated by adding 80 μl 10% trichloroacetic acid aqueous solution, followed by HPLC analysis.

For kinetic analysis, 1 μg of the recombinant protein was added to 150 μl of the assay buffer containing a saturated concentration (500 μM) of benzyl alcohol, isovanillyl alcohol, cinnamyl alcohol, vanillic alcohol, or ethanol, respectively, and varied concentrations of BA-CoA (3.9 μM to 500 μM). After 1 min at 28 °C, 80 μl 10% trichloroacetic acid aqueous solution was added to terminate the reaction. Reaction products were detected and quantified using UHPLC. Benzylbenzoate, ethyl benzoate and benzylcinnamate were quantified using standard curves generated from analytical standards. For other esters, quantification was based on monitoring the consumption of the corresponding alcohol.

Enzymatic characterization of OsBBH

Detached leaves were incubated with substrates for catalysis. Analysis was performed according to a previous report⁵³. In brief, *A. tumefaciens* strain GV3101 harbouring pEARLY100:35S-OsBBH and pEARLY100:35S-mVenus were infiltrated into different regions of the same *N. benthamiana* leaf. After 72 h, infiltrated leaves were collected for RNA extraction and subsequent expression level analysis. For metabolite analysis, approximately 0.02 g of the infiltrated leaves were collected and incubated in benzylbenzoate solution (200 μM benzylbenzoate dissolved in 0.01% Silwet-77) for 16 h. Then, the leaves were washed with de-ionized water, ground in liquid nitrogen, and homogenized in 0.5 ml methanol, with the addition of 173 ng phenethyl phenylacetate as internal standard. The supernatant was dried with nitrogen and dissolved in 150 μl 70% methanol, followed by extraction with 150 μl hexane. The hexane phase was collected for GC-MS analysis. All reactions in each batch of the experiments were conducted with five biologically independent samples.

Microsomal protein preparation and in vitro enzyme assays were conducted according to previous studies^{54,55}. In brief, pEARLY100:35S-OsBBH was transiently expressed in *N. benthamiana* leaves. Then, the microsomal proteins were prepared from *N. benthamiana* leaves and used for analysis. Leaves expressing pEARLY100:35S-mVenus were used as control. Approximately 0.5 g of *N. benthamiana* leaves were ground into fine powder in liquid nitrogen and then resuspended in 30 ml of microsome extraction buffer (50 mM tris-HCl, 2 mM EDTA, 2 mM 2-mercaptoethanol and 0.4 M sucrose, pH 7.4). The homogenate was incubated on ice for 20 min, followed by filtering through 2 layers of Miracloth (Millipore), and centrifuged at 10,000g for 10 min. The supernatant was collected for further centrifuged at 100,000g for 1 h. The resulting pellet was dissolved in 100 μl resuspension buffer (100 mM HEPES, pH 7.4). Microsome protein concentration was measured using a Bradford kit. For the BBH catalytic activity assay, 5–10 μg of microsomal proteins were added into 100 μl reaction buffer containing 50 mM HEPES (pH 7.4), 0.005% Silwet, 200 μM benzylbenzoate,

and 2 mM NADPH. After incubation in 28 °C for 1 h, 50 μl of internal standard solution containing 0.005% Silwet and 0.54 μg of phenethyl phenylacetate as internal standard was added and the mixture was extracted with 200 μl of ethyl acetate. The ethyl acetate phases were collected and analysed by GC-MS.

Enzymatic characterization of OsBSE

The esterase activity of OsBSE was analysed according to a previous report⁴³, with minor modifications. In brief, 150 μl buffer containing 50 mM Tris-HCl at pH 7.0 and 200 μM benzylsalicylate were mixed with 1 μg of purified proteins in 10 μl solution to start the enzymatic reaction. After 60 min at 28 °C, 80 μl 10% trichloroacetic acid aqueous solution was added to terminate the reaction. The solution was sent for analysis by HPLC.

For enzyme kinetic analysis, 1 μg recombinant protein were added to 150 μl assay buffer containing varied concentrations of benzylsalicylate, benzylbenzoate, or cinnamylbenzoate (3.9 μM to 500 μM). After 10 min at 28 °C, the reaction was terminated as mentioned. The content of SA or BA produced was analysed by UHPLC.

Extraction and enzymatic profiling of cytosolic and non-cytosolic protein fractions from rice leaves

Cytosolic and non-cytosolic protein fractions were extracted from four-week-old rice leaves using a modified protocol based on a previous report⁵⁶. In brief, 8 g of rice leaves were homogenized in ice-cold extraction buffer (50 ml, 0.5 M sorbitol, 20 mM HEPES, 10 mM KCl, 5 mM 2-mercaptoethanol, pH 7.0). The homogenate was filtered through two layers of Miracloth (Merck millipore) and centrifuged at 10,000g for 60 min. The supernatant was carefully collected as cytosolic fraction, while the precipitation was resuspended in 2 ml 50 mM Tris-HCl to obtain the non-cytosolic fraction. Protein concentrations in both fractions were determined using the Bradford kit (Coolaber, SK1060). For enzymatic analysis of BSE, the fractions containing 5 μg proteins were added into 150 μl buffer containing 500 μM benzylsalicylate and incubated at 28 °C for 5 min. The reaction products were analysed by UHPLC. The cytosolic fraction was verified by measuring alcohol dehydrogenase (ADH) activity, while the non-cytosolic fraction was confirmed by measuring catalase (CAT) activity and chlorophyll content⁵⁶. The ADH and CAT activities were measured using the ADH Assay Kit (Beyotime Biotechnology, S0241S) and the CAT Assay Kit (Beijing Solarbio Science & Technology, BC0200) following manufacturers' instructions. Chlorophyll contents were determined by measuring the absorbance at 649 nm and 665 nm. Concentrations of chlorophylls *a* and *b* were calculated using extinction coefficients as previously described⁵⁷. All absorbances were detected by a microplate reader (BioTek, Synergy H1, Agilent).

Extraction and immunoblotting of cytosolic and non-cytosolic protein fractions from rice protoplasts

Rice protoplasts expressing BSE-YFP and ER-mCherry were collected and homogenized in ice-cold extraction buffer, and the homogenate was then centrifuged at 10,000g for 60 min at 4 °C. The supernatant was carefully collected as the cytosolic fraction, while the pellet was resuspended in 50 mM Tris-HCl (pH 7.4) to obtain the non-cytosolic fraction. Protein concentrations in both fractions were determined using the Bradford kit (Coolaber, SK1060). Proteins were separated by SDS-PAGE and detected via immunoblotting using the following primary antibodies: anti-Histone H3 (1:5,000; ab1791, Abcam), anti-GAPDH (1:5,000; HRP-60004, Proteintech), anti-YFP/GFP (1:4,000; E-A02020, Abbkine), and anti-mCherry/RFP (1:5,000; ab65856, Abcam). Immunoblots were developed using the Super ECL Star chemiluminescent substrate (US Everbright). Images from immunoblotting were collected with Tanon-5200 Chemiluminescent Imaging System (Tanon Science and Technology).

Virus-induced gene silencing

VIGS in *S. lycopersicum* was conducted using the bipartite tobacco rattle virus (TRV) vectors, pTRV1 and pTRV2, according to a previous report⁵⁸. Putative orthologues of *OsBEBT*, *OsBBH* or *OsBSE* were selected as VIGS target genes. cDNA fragments (200–300 bp) of *SIBEBT* (*Solyc07g049660*), *SIBBH* (*Solyc03g122350*) and *SIBSE* (*Solyc02g069800*), amplified using primers listed in Supplementary Table 1, were inserted into the pTRV2 vector and transformed into *A. tumefaciens* strain GV3101. The empty pTRV2 vector was used as a negative control, while pTRV2 containing *SIPDS* (encoding phytoene desaturase) fragments was used as a positive control. *A. tumefaciens* GV3101 harbouring pTRV1 or pTRV2 were cultivated, resuspended in transformation buffer, and mixed in equal amount. Two-day-old tomato seedlings were soaked in the *Agrobacterium* suspension and subjected to vacuum infiltration.

VIGS of *TaBEBT*, *TaBBH*, and *TaBSE* in wheat seedlings was performed using barley stripe mosaic virus (BSMV) system as described^{59,60}. BSMV contains three positive-sense, single-stranded RNA segments (α , β and γ). The γ segment can be modified at the cDNA level to incorporate fragments of target genes for VIGS. Putative orthologous genes of *OsBEBT*, *OsBBH*, or *OsBSE* were selected as VIGS target genes. In brief, the highly conserved cDNA sequence fragments (200–300 bp) of *TaBEBT* homologues (*TraesCS1D03G0425100*, *TraesCS1D03G0424200*, *TraesCS1B03G0562000* and *TraesCS1A03G0468700*), *TaBBH* homologues (*TraesCS5D03G0509500*, *TraesCS5D03G0509300*, *TraesCS5B03G0555800*, *TraesCS5B03G0555700*, *TraesCS5A03G0546200* and *TraesCS5A03G0546100*) and *TaBSE* homologues (*TraesCS1D03G0617800*, *TraesCS1D03G0617300*, *TraesCS1B03G0749400*, *TraesCS1B03G0747800*, *TraesCS1A03G0660500* and *TraesCS1A03G0659500*) were inserted into the RNAY cDNA strand to prepare cDNA clones of BSMV:*TaBEBT*, BSMV:*TaBBH* or BSMV:*TaBSE*, respectively (primers and insertion sites are listed in Supplementary Table 1). The vector containing the *TaPDS* cDNA fragment was used as a positive control and the empty vector as a negative control. The RNAY, RNA β and RNAY-derived clones were linearized and the in vitro transcription was carried out in accordance with the Ribo MAXTM Large Scale RNA Production System-T7 kit and the Ribom7G Cap Analog kit (Promega, P1712). Then, the synthesized RNA transcripts of RNAY, RNA β and RNAY were mixed in equal molar ratios and diluted for inoculation onto wheat leaves at the two-leaf stage.

VIGS of *GhBEBT*, *GhBBH* and *GhBSE* in cotton seedlings was performed as described⁶¹. Putative orthologous genes of *OsBEBT*, *OsBBH* or *OsBSE* were selected as VIGS target genes. The highly conserved cDNA sequence fragments (200–300 bp) of *GhBEBT* (Gohir.D13G163100.1 and Gohir.A13G158400.1), *GhBBH* (Gohir.D11G140901.1 and Gohir.A11G134700.1), *GhBSE* (Gohir.D06G184200.1 and Gohir.A06G174100.1), amplified using primers listed in Supplementary Table 1, were inserted into the pTRV2 vector. An equal volume of *A. tumefaciens* GV3101 harbouring pTRV1 and different pTRV2 vectors were mixed and infiltrated into the cotyledons of two-week-old cotton seedlings. The empty pTRV2 vector served as a negative control, while pTRV2 containing a fragment of the cloroplastos alterados (*CLA*) gene was used as a positive control.

Putative orthologous genes of *OsBEBT*, *OsBBH* or *OsBSE* from different plants were obtained through reciprocal protein BLAST. Silencing efficiency in the above VIGS experiments was confirmed in the positive control group (plants with silenced *SIPDS*, *TaPDS* or *GhCLA*) by the appearance of an albino phenotype, which also indicated the appropriate time for collection or further pathogen infection experiments in the target gene-silenced groups.

Pathogen treatment

M. oryzae were cultivated in a growth chamber at 28 °C with a 16 h:8 h light:dark photoperiod for 10 days. Spores were collected and resuspended in 0.01% gelatin to make the concentration of 5×10^6 per ml.

For fungal biomass evaluation, young leaves from 4-leaf-stage rice were cut into evenly sized leaf segments and slightly scratched to facilitate inoculation. A 10 μ l aliquot of spore suspension were inoculated on each wound, and the leaf segments were incubated at 28 °C. Seven days post-inoculation, disease symptoms were measured using ImageJ 1.42q software (<https://imagej.nih.gov/ij/>), and the relative fungal biomass was calculated using DNA-based qPCR by measuring the level of the *M. oryzae* transposable element *MoPot2* relative to that of *OsUBIQUITIN*⁶².

The bacterial strain *Pseudomonas syringae* DC3000 was cultured in Luria–Marine liquid overnight. The following day, the bacteria were collected, washed with sterile water, and resuspended to reach the final concentration of 1×10^6 per ml. The bacteria were then inoculated into *Arabidopsis* leaves using a syringe, and the inoculated plants were kept under ambient humidity for approximately 1 h to allow for water evaporation before being transferred to a growth chamber⁵. Two days post-inoculation, *Arabidopsis* leaves were collected for PCR with reverse transcription (RT–PCR) and metabolite analysis.

For *S. lycopersicum* inoculation, freshly prepared DC3000 from the nutrient yeast glycerol agar (NYGA) plate containing 50 μ g ml⁻¹ rifampicin was resuspended in 10 mM MgCl₂ and 0.02% Silwet-77. OD₆₀₀ was adjusted to 0.01 before the solution was sprayed on tomato leaves. Leaves were collected for further analysis 24 h after inoculation.

F. graminearum for wheat pathogen infection was cultured on potato dextrose agar and grown at 28°C for 5 days before being inoculated into mung bean soup medium to induce spore production. After 7 days of growth in a shaking incubator at 28 °C, the conidia suspension of *F. graminearum* (1×10^5 per ml) was evenly sprayed on wheat leaves. Sterile distilled water was inoculated in the same way as the control. Two days after inoculation, the leaves were collected for RT–PCR and metabolite analysis.

Verticillium dahliae V991 for cotton pathogen infection was cultivated on potato dextrose agar for four days, and the spores were collected and grown in Czapek's liquid medium. Cotton seedlings were inoculated with spore suspensions (8×10^6 per ml) through injured roots. The leaves were collected three days after inoculation⁶¹.

Plant metabolite extraction

Extraction of plant SA and BA was performed according to a previous report²⁸ with minor modifications. In brief, ~100 mg of plant leaves was ground and added to 0.5 ml of ethyl acetate containing 2.5 ng deuterium-labelled SA (SA-d4, GLPBIO, GC49480), followed by vigorous shaking for 10 min. The samples were subsequently centrifuged for 10 min at 4 °C before the supernatant was collected. Then, 0.5 ml ethyl acetate containing 2.5 ng SA-d4 was added to the precipitate, followed by vigorous shaking for 10 min, and subsequently centrifuged for 10 min at 4 °C. The supernatants from the above two centrifugations were combined, vacuum evaporated, re-dissolved in 70% methanol, and transferred to an injection vial to be analysed by LC–MS/MS.

Extraction of plant SAG and SGE was performed according to a previous report⁶³ with minor modifications. In brief, around 100 mg of plant leaves was ground and added to 1 ml of 75% methanol containing 5 ng deuterium-labelled SA. The mixture was incubated at 4 °C for 12 h, followed by centrifugation at 12,000g for 10 min at 4 °C. The resulting supernatant was carefully collected and subjected to LC–MS/MS analysis for quantification.

Extraction of rice benzylbenzoate and benzylsalicylate was conducted as follows. Approximately 5 g of rice leaves were ground with nitrogen and added to 20 ml ethyl acetate containing 5 ng SA-d4, followed by sonification for 30 min. The samples were subsequently centrifuged for 10 min, and the supernatant was collected and vacuum vapoured. The concentrate was re-dissolved in 3 ml 70% methanol and extracted by 2.8 ml hexane. The hexane phase was collected and concentrated by nitrogen gas, and re-dissolved in 80 μ l methanol for LC–MS/MS analysis.

Article

Extraction of benzyl-CoA was performed as described⁶⁴. In brief, 200 mg of rice leaves were ground in liquid nitrogen, and resuspended with 300 µl of 10% TCA solution. Samples were centrifuged for 10 min at 4 °C, after which this extraction was repeated. Combined supernatants were mixed with an equal volume of 8% ammonium acetate solution, then centrifuged to precipitate residual impurities. Solid-phase extraction (SPE) cartridges (1 cc, 50 mg, C18 Sep Pak Vac, Waters) were preconditioned with 2 ml methanol, 2 ml ultrapure water, and 2 ml 4% ammonium acetate in 5% TCA. Samples were loaded to the columns and washed with 2 ml 4% ammonium acetate. Columns were flushed with air and eluted with 200 µl of 80% isopropanol and 20% ethyl acetate. The elution was collected for LC–MS/MS analysis.

HPLC analysis

For initial enzyme activity test, the substrates and products of OsBEBT, OsBSE, and OsTE were detected by HPLC (Shimadzu LC-20A) equipped with a Photo-diode array at a wavelength of 210 nm. Samples were separated with a Welch Ultimate XB-C18 column (250 × 4.6 mm, 5 µm particle size). For each run, 20 µl of each sample were injected into a column at 30 °C. The mobile phase consisted of solvent A (0.1% phosphoric acid in distilled water) and solvent B (acetonitrile) with a flow rate of 1 ml min⁻¹. A gradient elution program was used as follows: 0–20 min, 80% to 20% A; and 20–25 min, 20% to 0% A.

UHPLC analysis

For kinetics analysis, the enzymatic products of *OsBEBT*, *OsBSE* and *OsTE* were quantified by UHPLC (Vanquish Flex, Thermo Fisher Scientific) equipped with a variable wavelength detector or a fluorescence detector. Samples were separated with a Sepax HP-C18 column (2.1 mm × 150 mm, 3 µm particle size) maintained at 40 °C. For each run, 10 µl of each sample were injected into a column at 25 °C. The mobile phase consisted of solvent A (HPLC-grade methanol) and solvent B (distilled H₂O with 0.1% formic acid) with a flow rate of 0.5 ml min⁻¹. A gradient elution program was used as follows: 0–1 min, 95% B; 1–8 min, 95% to 50% B; 8–10 min, 50% to 0% B; 10–15 min, 0% B; 15–15.5 min, 0% to 95% B; and 15.5–19 min, 95% B. SA was detected by the fluorescence detector, with the excitation wavelength of 295 nm and emission wavelength of 400 nm. The wavelengths for the detection of benzylbenzoate and other chemicals were 194 nm and 210 nm. Quantification of the detected products was performed using standard curves for BA, benzylbenzoate, benzylsalicylate, cinnamic acid and SA based on UV or visible light absorbance.

LC–MS/MS with MRM analysis

LC–MS/MS analysis was performed utilizing an ExionLC HPLC system coupled with an AB SCIEX QTRAP 6500plus mass spectrometer. Aliquots of 2 µl were injected into an Acquity BEH C18 column (2.1 × 50 mm). Chromatographic separation was achieved with a flow rate of 0.4 ml min⁻¹, using 0.1% formic acid in water (solvent A) and acetonitrile (solvent B). Liquid chromatography separation was performed using an 8-min linear elution gradient: 0 min, 5% B; 1.5 min, 20% B; 3.5 min, 50% B; 5 min, 90% B; 5–6.5 min, 90% B; 6.6 min, 5% B; and 6.6–8 min, 5% B. BA, SA, SAG, SGE and deuterium-labelled SA (SA-d4, GLPBIO, GC49480) were analysed in negative ion-mode electrospray ionization (ESI–), while benzylbenzoate, benzylsalicylate, deuterium-labelled benzylbenzoate and deuterium-labelled benzylsalicylate was analysed in positive ion-mode (ESI+). MRM mode quantification settings were: curtain gas at 35 psi; ion spray voltage at -4.5 kV for ESI– and +5.5 kV for ESI+; ion source temperature at 500 °C; ion source gases 1 and 2 at 60 and 40 psi, respectively. MRM transitions were set at 121.0/77.0 for BA, 137.0/93.0 for SA, 141.0/97.0 for SA-d4, 299.2/137.2 for SAG, 299.2/150.9 for SGE, 229.1/91.1 for benzylsalicylate, and 213.0/91.0 for benzylbenzoate, 240.1/98.1 for deuterium-labelled benzylsalicylate, 223.1/96.1 for deuterium-labelled benzylbenzoate. Declustering potential and collision energy values were -30 V/-17 V

for BA, -35 V/-21 V for SA, -60 V/-16 V for SAG, -60 V/-30 V for SGE, -35 V/-20 V for SA-d4, 50 V/33 V for benzylsalicylate, and 50 V/26 V for benzylbenzoate, 50 V/33 V for deuterium-labelled benzylsalicylate, 50 V/26 V for deuterium-labelled benzylbenzoate. A 20 ms dwell time was applied. Quantification was performed using standard curves established with analytical standards and a 5 ng ml⁻¹ SA-d4 internal standard.

For benzoyl-CoA detection, the ExionLC HPLC system coupled with an AB Sciex QTrap 6500plus mass spectrometer was used. Aliquots of 2 µl were injected into an Acquity BEH Amide column (2.1 × 50 mm). Chromatographic separation was achieved with a flow rate of 0.4 ml min⁻¹, with 10 mM ammonium acetate and 0.05% ammonium hydroxide in water (solvent A) and 10 mM ammonium acetate and 0.05% ammonium hydroxide in 90% acetonitrile (solvent B). An 8-min linear gradient was employed for elution. The gradient program was as follows: 0–1 min, 95% B; 1–2.5 min, 95% to 55% B; 2.5–5 min, 55% B; 5–5.1 min, 55% to 95% B; and 5.1–8 min, 95% B. Benzoyl-CoA and deuterium-labelled benzoyl-CoA were analysed in positive ion-mode (ESI+). MRM mode quantification settings were: curtain gas at 40 psi; ion spray voltage at +4.5 kV for ESI+; ion source temperature at 500 °C; ion source gases 1 and 2 at 55 and 50 psi, respectively. MRM transitions were set at 872.2/365.0 for benzoyl-CoA, 877.2/370.0 for deuterium-labelled benzoyl-CoA. Declustering potential and collision energy values were 100 V/47 V for benzoyl-CoA, and 100 V/47 V for deuterium-labelled benzoyl-CoA. A 100 ms dwell time was applied with quantification using a standard curve established with analytical standards.

GC–MS analysis

One microlitre sample was auto-injected onto Agilent GC 8890 equipped with an HP-5MS capillary column and an Agilent 5977B MS detector. Temperature of the gas chromatography oven was programmed as follows: initial hold at 45 °C for 2 min, followed by sequential increases of 10 °C/min to 90 °C, 3 °C/min to 105 °C, and 10 °C/min to 280 °C, with a final hold at 280 °C for 7 min. Mass spectra were acquired in scan mode (35–300 m/z) for qualitative analysis or selected ion monitoring (SIM) mode (m/z = 91, 104, 212, 228) for quantitative analysis. The peak area of the EIC at m/z = 228 was used to quantify benzylsalicylate, while the peak area of EIC at m/z = 104 was used to quantify phenethyl phenylacetate. The response factor of benzylsalicylate relative to phenethyl phenylacetate was determined using standard curves generated from authentic standards and applied for the quantification of benzylsalicylate.

Phylogenetic analysis

Rice protein sequences were downloaded from the Rice Annotation Project Database (RAP-DB)⁶⁵ and those of *N. tabacum* were retrieved from NCBI (GCF_000715135.1⁶⁶). Homologues of each gene were identified using DIAMOND⁶⁷ v2.0.14, with the query gene and an e-value threshold of 10⁻¹⁰. The identified sequences were aligned using MAFFT⁶⁸ v7.490, and poorly aligned regions were trimmed using TrimAI⁶⁹ v1.4. A maximum likelihood phylogenetic tree was constructed using IQ-TREE⁷⁰ v2.3.0 with the “LG + F + G4” model and 1,000 ultrafast bootstrap replicates⁷¹.

Gene co-expression analysis

ATTED-II (<https://atted.jp>), a gene co-expression resource based on publicly available RNA-sequencing and microarray data⁷², was used to identify genes co-expressed with *OsCNL1* (Entrez Gene ID: 4331500). *OsCNL1* was queried in the ATTED-II database (<https://atted.jp/top-search/#CoExSearch>), and the top 2,000 co-expressed genes were ranked based on their z-scores, which indicate co-expression strength. These genes were visualized around *OsCNL1* using the Cytoscape software (v.3.7.2), with their distance to *OsCNL1* reflecting the strength of co-expression.

Statistical analysis and reproducibility

Statistical significance was assessed by two-tailed Student's *t*-tests (for pairwise comparisons) or one-way ANOVA with Tukey's HSD post hoc test. When the assumption of equal variances was violated (as determined by Bartlett's test), Welch's ANOVA with Games–Howell post hoc tests was applied. All statistical analyses were performed using GraphPad Prism 8.0 (<https://www.graphpad.com/>). Kinetic parameters were derived by fitting data to the Michaelis–Menten equation using nonlinear regression in the same software. Specific statistical tests and sample sizes are indicated in the respective figure legends. Sample sizes were not predetermined using statistical methods. Most experiments were performed with at least three biological replicates, which is the minimum number required for robust statistical analysis of metabolite data and sufficient to assess experimental variability. For specialized experiments, such as VIGS and tobacco transient expression, three to six replicates were used to ensure the reliability of the results. Sample allocation was random. Blinding was not used in this study.

For immunoblot analysis, fluorescence microscope analysis and semi-quantitative RT–PCR analysis, representative images were shown and each experiment was independently repeated at least three times with similar results to ensure reproducibility.

Reporting summary

Further information on research design is available in the Nature Portfolio Reporting Summary linked to this article.

Data availability

All data associated with this study are provided. The full versions of all images of gels and immunoblots are provided in the Supplementary Fig. 1. The accession numbers of all genes cloned or experimentally analysed in this study are shown in the Supplementary Tables 1 and 2. Sequence data related to these genes can be found in the GenBank/EMBL data libraries. Gene co-expression data can be accessed from the ATTED-II database (https://atted.jp/top_search/#CoExSearch) and are also provided within the Source Data file. The source data for all graphs are available in the Source Data files. The gene expression data presented in Extended Data Fig. 10 can be obtained from the NCBI Sequence Read Archive (SRA) database (<https://www.ncbi.nlm.nih.gov/sra>) using the BioProject accession numbers indicated in the figure, and are also provided in the Source Data.

51. Huang, X. Q., Li, R., Fu, J. & Dudareva, N. A peroxisomal heterodimeric enzyme is involved in benzaldehyde synthesis in plants. *Nat. Commun.* **13**, 1352 (2022).
52. Chen, Y. et al. Nuclear translocation of OsmFT1 that is impeded by OsTIP1 promotes drought tolerance in rice. *Mol. Plant* **14**, 1297–1311 (2021).
53. Jinkerson, R. E. et al. Biosynthesis of chlorophyll c in a dinoflagellate and heterologous production in planta. *Curr. Biol.* **34**, 594–605.e4 (2024).
54. Gou, M. et al. Cytochrome *b*₆ is an obligate electron shuttle protein for syringyl lignin biosynthesis in *Arabidopsis*. *Plant Cell* **31**, 1344–1366 (2019).
55. Clausen, M. et al. The bifurcation of the cyanogenic glucoside and glucosinolate biosynthetic pathways. *Plant J.* **84**, 558–573 (2015).
56. Conart, C. et al. A cytosolic bifunctional geranyl/farnesyl diphosphate synthase provides MVA-derived GPP for geraniol biosynthesis in rose flowers. *Proc. Natl. Acad. Sci. USA* **120**, e2221440120 (2023).
57. Porra, R. J., Thompson, W. A. & Kriedemann, P. E. Determination of accurate extinction coefficients and simultaneous equations for assaying chlorophylls *a* and *b* extracted with four different solvents: verification of the concentration of chlorophyll standards by atomic absorption spectroscopy. *Biochim. Biophys. Acta* **975**, 384–394 (1989).
58. Ding, S. et al. Phytosulfokine peptide optimizes plant growth and defense via glutamine synthetase GS2 phosphorylation in tomato. *EMBO J.* **42**, e111858 (2023).
59. He, X. et al. HvEXPB7, a novel β -expansin gene revealed by the root hair transcriptome of Tibetan wild barley, improves root hair growth under drought stress. *J. Exp. Bot.* **66**, 7405–7419 (2015).
60. Zhang, P. et al. Functional analysis of *Tadhn1312* by virus-induced gene silencing (VIGS) in common wheat (*Triticum aestivum* L.). *Mol. Plant Breed.* <https://doi.org/10.5376/mpb.2020.11.0002> (2020).
61. Sun, Y. et al. GoPGS regulates cotton pigment gland size and contributes to biotic stress tolerance through jasmonic acid pathways. *New Phytol.* **243**, 839–845 (2024).
62. Wang, J. et al. Two VOZ transcription factors link an E3 ligase and an NLR immune receptor to modulate immunity in rice. *Mol. Plant* **14**, 253–266 (2021).
63. Hu, Y. et al. Salicylic acid carboxyl glucosyltransferase UGT87E7 regulates disease resistance in *Camellia sinensis*. *Plant Physiol.* **188**, 1507–1520 (2022).
64. Quale, A. V., Cooper, B. R. & Dudareva, N. Profiling hydroxycinnamoyl-coenzyme A thioesters: unlocking the back door of phenylpropanoid metabolism. *Anal. Biochem.* **420**, 182–184 (2012).
65. Sakai, H. et al. Rice Annotation Project Database (RAP-DB): an integrative and interactive database for rice genomics. *Plant Cell Physiol.* **54**, e6 (2013).
66. Sierra, N. et al. The tobacco genome sequence and its comparison with those of tomato and potato. *Nat. Commun.* **5**, 3833 (2014).
67. Buchfink, B., Xie, C. & Huson, D. H. Fast and sensitive protein alignment using DIAMOND. *Nat. Methods* **12**, 59–60 (2015).
68. Katoh, K. & Standley, D. M. MAFFT multiple sequence alignment software version 7: improvements in performance and usability. *Mol. Biol. Evol.* **30**, 772–780 (2013).
69. Capella-Gutiérrez, S., Silla-Martínez, J. M. & Gabaldón, T. trimAl: a tool for automated alignment trimming in large-scale phylogenetic analyses. *Bioinformatics* **25**, 1972–1973 (2009).
70. Minh, B. Q. et al. IQ-TREE 2: new models and efficient methods for phylogenetic inference in the genomic era. *Mol. Biol. Evol.* **37**, 1530–1534 (2020).
71. Hoang, D. T., Chernomor, O., Von Haeseler, A., Minh, B. Q. & Vinh, L. S. UFBoot2: improving the ultrafast bootstrap approximation. *Mol. Biol. Evol.* **35**, 518–522 (2018).
72. Obayashi, T., Hibara, H., Kagaya, Y., Aoki, Y. & Kinoshita, K. ATTED-II v11: a plant gene coexpression database using a sample balancing technique by subbagging of principal components. *Plant Cell Physiol.* **63**, 869–881 (2022).
73. Huang, W., Wang, Y., Li, X. & Zhang, Y. Biosynthesis and regulation of salicylic acid and *N*-hydroxypiperolic acid in plant immunity. *Molecular Plant* **13**, 31–41 (2020).
74. Zhang, Y. & Li, X. Salicylic acid: biosynthesis, perception, and contributions to plant immunity. *Curr. Opin. Plant Biol.* **50**, 29–36 (2019).
75. Peng, Y., Yang, J., Li, X. & Zhang, Y. Salicylic acid: biosynthesis and signaling. *Annu. Rev. Plant Biol.* **72**, 761–791 (2021).
76. Rossi, C. A. M., Marchetta, E. J. R., Kim, J. H. & Castroverde, C. D. M. Molecular regulation of the salicylic acid hormone pathway in plants under changing environmental conditions. *Trends Biochem. Sci.* **48**, 699–712 (2023).
77. Klämbt, H. D. Conversion in plants of benzoic acid to salicylic acid and its β -glucoside. *Nature* **196**, 491–491 (1962).
78. el-Basyouni, S. Z., Chen, D., Ibrahim, R. K., Neish, A. C. & Towers, G. H. N. The biosynthesis of hydroxybenzoic acids in higher plants. *Phytochemistry* **3**, 485–492 (1964).
79. Yalpani, N., Leon, J., Lawton, M. A. & Raskin, I. Pathway of salicylic acid biosynthesis in healthy and virus-inoculated tobacco. *Plant Physiol.* **103**, 315–321 (1993).
80. Ribicky, D. M., Shulav, V. & Raskin, I. Intermediates of salicylic acid biosynthesis in tobacco. *Plant Physiol.* **118**, 565–572 (1998).
81. Chadha, K. C. & Brown, S. A. Biosynthesis of phenolic acids in tomato plants infected with *Agrobacterium tumefaciens*. *Can. J. Bot.* **52**, 2041–2047 (1974).
82. Coquoz, J. L., Buchala, A. & Metraux, J. P. The biosynthesis of salicylic acid in potato plants. *Plant Physiol.* **117**, 1095–1101 (1998).
83. Meuwly, P., Molders, W., Buchala, A. & Metraux, J. P. Local and systemic biosynthesis of salicylic acid in infected cucumber plants. *Plant Physiol.* **109**, 1107–1114 (1995).
84. Guo, Y. et al. Blue light enhances health-promoting sulforaphane accumulation in broccoli (*Brassica oleracea* var. *italica*) sprouts through inhibiting salicylic acid synthesis. *Plants* **12**, 3151 (2023).
85. Lastochkina, O. et al. Role of endogenous salicylic acid as a hormonal intermediate in the bacterial endophyte *Bacillus subtilis*-induced protection of wheat genotypes contrasting in drought susceptibility under dehydration. *Plants* **11**, 3365 (2022).
86. Wang, Y., Wen, T., Huang, Y., Guan, Y. & Hu, J. Salicylic acid biosynthesis inhibitors increase chilling injury to maize (*Zea mays* L.) seedlings. *Plant Growth Regul.* **86**, 11–21 (2018).
87. Liu, N. et al. Salicylic acid alleviates aluminum toxicity in soybean roots through modulation of reactive oxygen species metabolism. *Front. Chem.* **5**, 96 (2017).
88. Dong, C.-J., Li, L., Shang, Q.-M., Liu, X.-Y. & Zhang, Z.-G. Endogenous salicylic acid accumulation is required for chilling tolerance in cucumber (*Cucumis sativus* L.) seedlings. *Planta* **240**, 687–700 (2014).
89. Zhou, X. & Zhong, J.-H. Intracellular salicylic acid is involved in signal cascade regulating low ammonium-induced taxoid biosynthesis in suspension cultures of *Taxus chinensis*. *Appl. Microbiol. Biotechnol.* **90**, 1027–1036 (2011).
90. Sawada, H., Shim, I.-S. & Usui, K. Induction of benzoic acid 2-hydroxylase and salicylic acid biosynthesis—modulation by salt stress in rice seedlings. *Plant Science* **171**, 263–270 (2006).
91. Pan, Q. et al. Salicylic acid synthesized by benzoic acid 2-hydroxylase participates in the development of thermotolerance in pea plants. *Plant Sci.* **171**, 226–233 (2006).
92. Kim, D. S. & Hwang, B. K. An important role of the pepper phenylalanine ammonia-lyase gene (PAL1) in salicylic acid-dependent signalling of the defence response to microbial pathogens. *J. Exp. Bot.* **65**, 2295–2306 (2014).
93. Pallas, J. A., Paiva, N. L., Lamb, C. & Dixon, R. A. Tobacco plants epigenetically suppressed in phenylalanine ammonia-lyase expression do not develop systemic acquired resistance in response to infection by tobacco mosaic virus. *Plant J.* **10**, 281–293 (1996).

Acknowledgements The authors thank X. Dong for helpful suggestions; S. Lu, M. Fang and X. Wu for assistance in HPLC measurement and data interpretation; W. Xia for assistance in UHPLC measurements and data interpretation; X. Zhao for sharing the endoplasmic reticulum marker; X.-Q. Huang for technical support in benzoyl ester analysis; and C. Song and Q. Wang for supplying SAG standard. This work was supported by the National Key Research and Development Program (2022YFD1401600 and 2024YFD1200401 to R.P. and 2024YFD2001003 to P.F.), the National Natural Science Foundation of China (32200231 and 32470287 to R.P. and 32472718 to P.F.), the Zhejiang Provincial Natural Science Foundation of China (LZ23C020002 to R.P. and LZ22C150005 to P.F.), the Natural Science Foundation of

Article

Hangzhou (2024S2RYBC130003 to R.P.), fellowship from the China National Postdoctoral Program for Innovative Talents (BX20230322 to Shuyan Song), fellowship of the China Postdoctoral Science Foundation (2023M743091 to Shuyan Song), Scientific Research Innovation Capability Support Project for Young Faculty (ZYGXQNJSKYCXNLZCXM-A12 to X.S.), and the Starry Night Science Fund of Zhejiang University Shanghai Institute for Advanced Study (SN-ZJU-SIAS-0011 to P.F.).

Author contributions R.P. and P.F. conceptualized and supervised the study. J. Yu participated in supervision and contributed resources. Y.W., R.P., P.F., W. Zhang and Shuyan Song designed the experiments, analysed the data and prepared the figures. Y.W. and M.K. conducted the molecular, genetic, physiological and biochemical experiments. Y.F., M.T., Y.Z. and X.S. performed the bioinformatic analysis. W. Zhang, Shuyan Song, X.C., J.C., J.P., H.D. and S.F. participated in the mass spectrometry analysis. Q.D., W. Zhu, L.Y., Xinyu Wang, Shiyong Song and Xiaowen Wang performed mutant preparation and protein localization analysis. C.Z., J.

Yang, T.Z. and F.C., participated in VIGS experiments. Q.Z. and Z.T. participated in rice pathogen inoculation experiments. J.H., P.C. and X.S. participated in data analysis. Y.W., Shuyan Song, R.P., P.F., J. Yu, R.L.L. and J.H. cowrote the manuscript.

Competing interests The authors declare no competing interests.

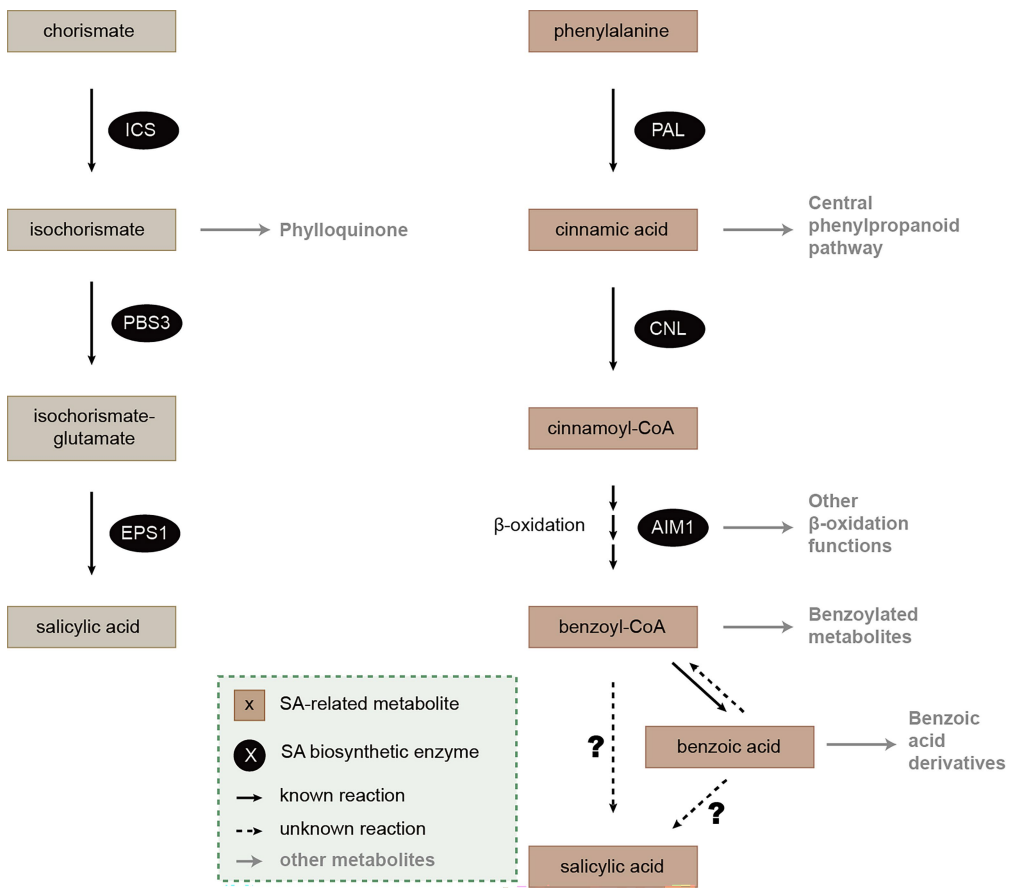
Additional information

Supplementary information The online version contains supplementary material available at <https://doi.org/10.1038/s41586-025-09280-9>.

Correspondence and requests for materials should be addressed to Pengxiang Fan or Ronghui Pan.

Peer review information *Nature* thanks Jing-Ke Weng and the other, anonymous, reviewer(s) for their contribution to the peer review of this work.

Reprints and permissions information is available at <http://www.nature.com/reprints>.



Extended Data Fig. 1 | Current understanding of plant SA biosynthetic pathways. Schematics of the two established SA biosynthetic routes: the isochorismate synthase (ICS) pathway (left) and the phenylalanine

ammonia-lyase (PAL) pathway (right)^{1,47,73–76}. Unknown steps in SA biosynthesis are marked with question marks. Related metabolic pathways sharing common precursors and enzymes are shown in grey.

Article

a

Plant group	Species	Method	Radiolabeled precursor	Radiolabeled SA	Reference
Monocot	<i>Oryza sativa</i>	Isotope tracking	cinnamic acid	Yes	Silverman <i>et al.</i> , Plant Physiology (1995)
Monocot	<i>Oryza sativa</i>	Isotope tracking	benzoic acid	Yes	Silverman <i>et al.</i> , Plant Physiology (1995)
Monocot	<i>Oryza sativa</i>	Isotope tracking	benzoic acid	Yes	Zou <i>et al.</i> , Journal of Agricultural and Food Chemistry (2024)
Dicot	<i>Primula acaulis</i>	Isotope tracking	phenylalanine	Yes	el-Basyouni <i>et al.</i> , Phytochemistry (1964)
Dicot	<i>Primula acaulis</i>	Isotope tracking	benzoic acid	Yes	el-Basyouni <i>et al.</i> , Phytochemistry (1964)
Dicot	<i>Gaultheria procumbens</i>	Isotope tracking	cinnamic acid	Yes	el-Basyouni <i>et al.</i> , Phytochemistry (1964)
Dicot	<i>Gaultheria procumbens</i>	Isotope tracking	benzoic acid	Yes	el-Basyouni <i>et al.</i> , Phytochemistry (1964)
Dicot	<i>Nicotiana tabacum</i>	Isotope tracking	cinnamic acid	Yes	Yalpani <i>et al.</i> , Plant Physiology (1993)
Dicot	<i>Nicotiana tabacum</i>	Isotope tracking	benzoic acid	Yes	Yalpani <i>et al.</i> , Plant Physiology (1993)
Dicot	<i>Nicotiana tabacum</i>	Isotope tracking	phenylalanine	Yes	Ribnicky <i>et al.</i> , Plant Physiology (1998)
Dicot	<i>Nicotiana tabacum</i>	Isotope tracking	benzoic acid	Yes	Zou <i>et al.</i> , Journal of Agricultural and Food Chemistry (2024)
Dicot	<i>Solanum tuberosum</i>	Isotope tracking	phenylalanine	Yes	Coquoz <i>et al.</i> , Plant Physiology (1998)
Dicot	<i>Solanum tuberosum</i>	Isotope tracking	cinnamic acid	Yes	Coquoz <i>et al.</i> , Plant Physiology (1998)
Dicot	<i>Solanum tuberosum</i>	Isotope tracking	benzoic acid	Yes	Coquoz <i>et al.</i> , Plant Physiology (1998)
Dicot	<i>Solanum tuberosum</i>	Isotope tracking	benzoic acid	Yes	Klåmbt <i>et al.</i> , Nature (1962)
Dicot	<i>Solanum lycopersicum</i>	Isotope tracking	phenylalanine	Yes	Zou <i>et al.</i> , Journal of Agricultural and Food Chemistry (2024)
Dicot	<i>Solanum lycopersicum</i>	Isotope tracking	benzoic acid	Yes	Zou <i>et al.</i> , Journal of Agricultural and Food Chemistry (2024)
Dicot	<i>Solanum lycopersicum</i>	Isotope tracking	cinnamic acid	Yes	Chadha <i>et al.</i> , Canadian Journal of Botany (1974)
Dicot	<i>Solanum lycopersicum</i>	Isotope tracking	benzoic acid	Yes	Chadha <i>et al.</i> , Canadian Journal of Botany (1974)
Dicot	<i>Cucumis sativus</i>	Isotope tracking	phenylalanine	Yes	Meuwly <i>et al.</i> , Plant Physiology (1995)
Dicot	<i>Cucumis sativus</i>	Isotope tracking	benzoic acid	Yes	Meuwly <i>et al.</i> , Plant Physiology (1995)
Dicot	<i>Camellia sinensis</i>	Isotope tracking	phenylalanine	Yes	Zou <i>et al.</i> , Journal of Agricultural and Food Chemistry (2024)
Dicot	<i>Camellia sinensis</i>	Isotope tracking	benzoic acid	Yes	Zou <i>et al.</i> , Journal of Agricultural and Food Chemistry (2024)
Dicot	<i>Glycine max</i>	Isotope tracking	phenylalanine	Yes	Zou <i>et al.</i> , Journal of Agricultural and Food Chemistry (2024)
Dicot	<i>Glycine max</i>	Isotope tracking	benzoic acid	Yes	Zou <i>et al.</i> , Journal of Agricultural and Food Chemistry (2024)
Dicot	<i>Fragaria ananassa</i>	Isotope tracking	phenylalanine	Yes	Zou <i>et al.</i> , Journal of Agricultural and Food Chemistry (2024)
Dicot	<i>Fragaria ananassa</i>	Isotope tracking	benzoic acid	Yes	Zou <i>et al.</i> , Journal of Agricultural and Food Chemistry (2024)
Dicot	willow (<i>Salix</i>)	Isotope tracking	phenylalanine	Yes	Zou <i>et al.</i> , Journal of Agricultural and Food Chemistry (2024)
Dicot	willow (<i>Salix</i>)	Isotope tracking	benzoic acid	Yes	Zou <i>et al.</i> , Journal of Agricultural and Food Chemistry (2024)
Dicot	<i>Helianthus annuus</i>	Isotope tracking	benzoic acid	Yes	Klåmbt <i>et al.</i> , Nature (1962)
Dicot	<i>Pisum sativum</i>	Isotope tracking	benzoic acid	Yes	Klåmbt <i>et al.</i> , Nature (1962)

b

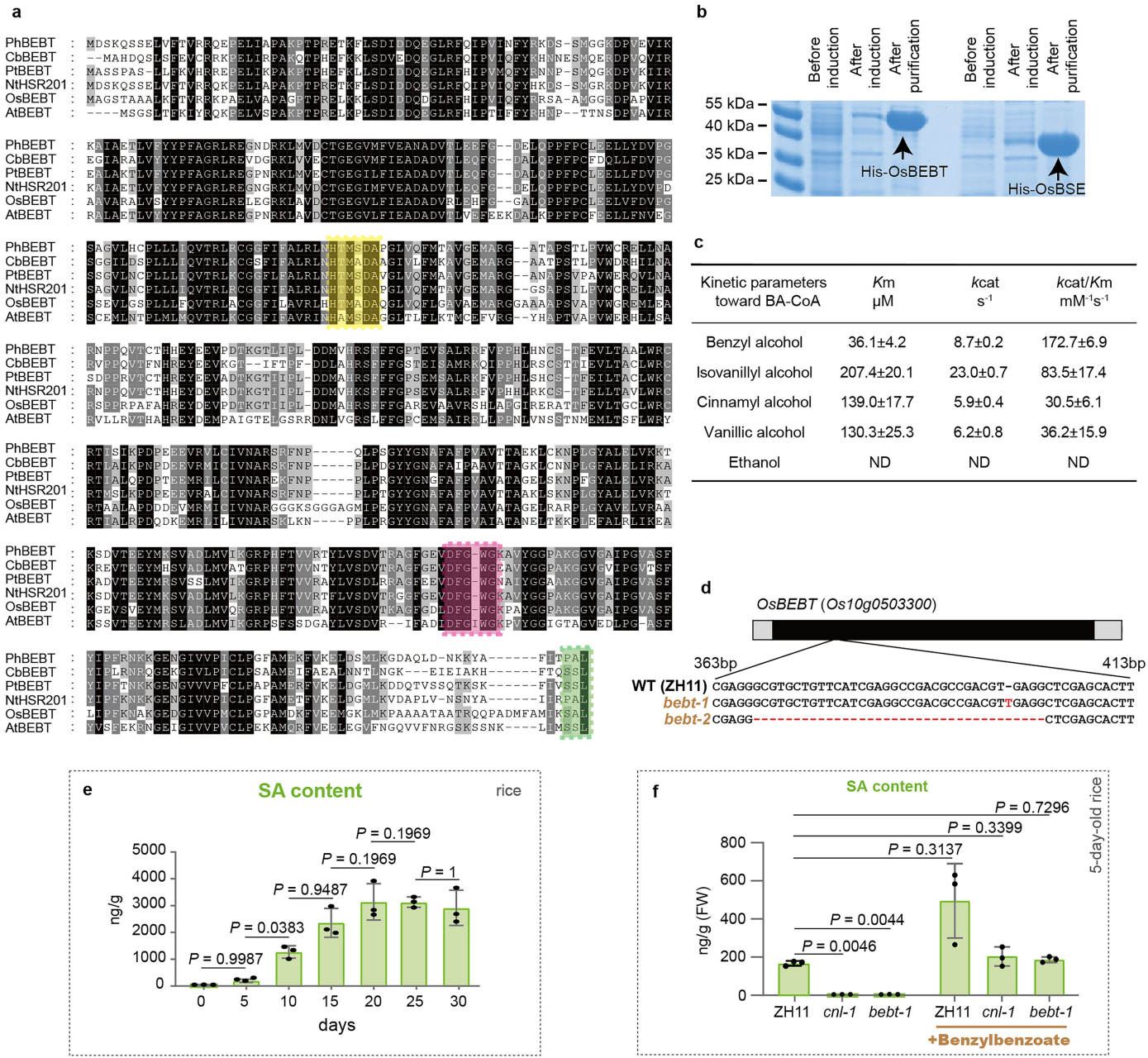
Plant group	Species	Method	Inhibited Enzyme	Decrease of SA	Reference
Gymnosperm	<i>Taxus chinensis</i>	Chemical inhibition	PAL	Yes	Zhou <i>et al.</i> , Applied Microbiology and Biotechnology (2011)
Gymnosperm	<i>Taxus chinensis</i>	Chemical inhibition	cytochrome P450	Yes	Zhou <i>et al.</i> , Applied Microbiology and Biotechnology (2011)
Monocot	<i>Triticum aestivum</i>	Chemical inhibition	cytochrome P450	Yes	Lastochkina <i>et al.</i> , Plants (2022)
Monocot	<i>Zea mays</i>	Chemical inhibition	PAL	Yes	Wang <i>et al.</i> , Plant Growth Regulation (2018)
Monocot	<i>Zea mays</i>	Chemical inhibition	cytochrome P450	Yes	Wang <i>et al.</i> , Plant Growth Regulation (2018)
Monocot	<i>Oryza sativa</i>	Chemical inhibition	cytochrome P450	Yes	Sawada <i>et al.</i> , Plant Science (2006)
Monocot	<i>Oryza sativa</i>	Chemical inhibition	cytochrome P450	Yes	Wang <i>et al.</i> , Developmental Cell (2024)
Dicot	<i>Cucumis sativus</i>	Chemical inhibition	PAL	Yes	Meuwly <i>et al.</i> , Plant Physiology (1995)
Dicot	<i>Cucumis sativus</i>	Chemical inhibition	PAL	Yes	Dong <i>et al.</i> , Planta (2014)
Dicot	<i>Cucumis sativus</i>	Chemical inhibition	cytochrome P450	Yes	Dong <i>et al.</i> , Planta (2014)
Dicot	<i>Brassica oleracea</i>	Chemical inhibition	cytochrome P450	Yes	Guo <i>et al.</i> , Plants (2023)
Dicot	<i>Nicotiana tabacum</i>	Chemical inhibition	cytochrome P450	Yes	León <i>et al.</i> , Proceedings of the National Academy of Sciences (1995)
Dicot	<i>Glycine max</i>	Chemical inhibition	cytochrome P450	Yes	Liu <i>et al.</i> , Frontiers in Chemistry (2017)
Dicot	<i>Solanum tuberosum</i>	Chemical inhibition	PAL	Yes	Coquoz <i>et al.</i> , Plant Physiology (1998)
Dicot	<i>Camellia sinensis</i>	Chemical inhibition	PAL	Yes	Zou <i>et al.</i> , Journal of Agricultural and Food Chemistry (2024)
Dicot	<i>Camellia sinensis</i>	Chemical inhibition	cytochrome P450	Yes	Zou <i>et al.</i> , Journal of Agricultural and Food Chemistry (2024)
Dicot	<i>Pisum sativum</i>	Chemical inhibition	PAL	Yes	Pan <i>et al.</i> , Plant Science (2006)
Dicot	<i>Pisum sativum</i>	Chemical inhibition	cytochrome P450	Yes	Pan <i>et al.</i> , Plant Science (2006)

c

Plant group	Species	Method	Disrupted Gene	Decrease of SA	References
Green alga	<i>Chlamydomonas reinhardtii</i>	Gene silencing	AIM1	Yes	Jia <i>et al.</i> , Molecular Plant (2023)
Monocot	<i>Aegilops variabilis</i>	Gene silencing	PAL	Yes	Zhang <i>et al.</i> , The Plant Journal (2021)
Monocot	<i>Oryza sativa</i>	Null mutant	PAL6	Yes	Duan <i>et al.</i> , Physiologia Plantarum (2014)
Monocot	<i>Oryza sativa</i>	Gene silencing	PAL	Yes	He <i>et al.</i> , PNAS (2020)
Dicot	<i>Nicotiana tabacum</i>	Gene silencing	PAL	Yes	Pallas <i>et al.</i> , The Plant Journal (1996)
Dicot	<i>Capsicum annuum</i>	Gene silencing	PAL	Yes	Kim <i>et al.</i> , Journal of Experimental Botany (2014)
Dicot	<i>Nicotiana tabacum</i>	Gene silencing	KAT	Yes	Kotera <i>et al.</i> , Plant and Cell Physiology (2023)
Dicot	<i>Nicotiana tabacum</i>	Gene silencing	CHD (AIM1)	Yes	Kotera <i>et al.</i> , Plant and Cell Physiology (2023)
Dicot	<i>Glycine max</i>	Gene silencing	PAL	Yes	Shine <i>et al.</i> , New Phytologist (2016)

Extended Data Fig. 2 | Summary of studies on SA biosynthesis in different plant species. (a) Heavy isotope labeling experimental evidence and conclusions of phenylalanine-derived SA biosynthesis^{4,44,77–83}. (b) Inhibitor-based experimental evidence and conclusions of phenylalanine-derived SA

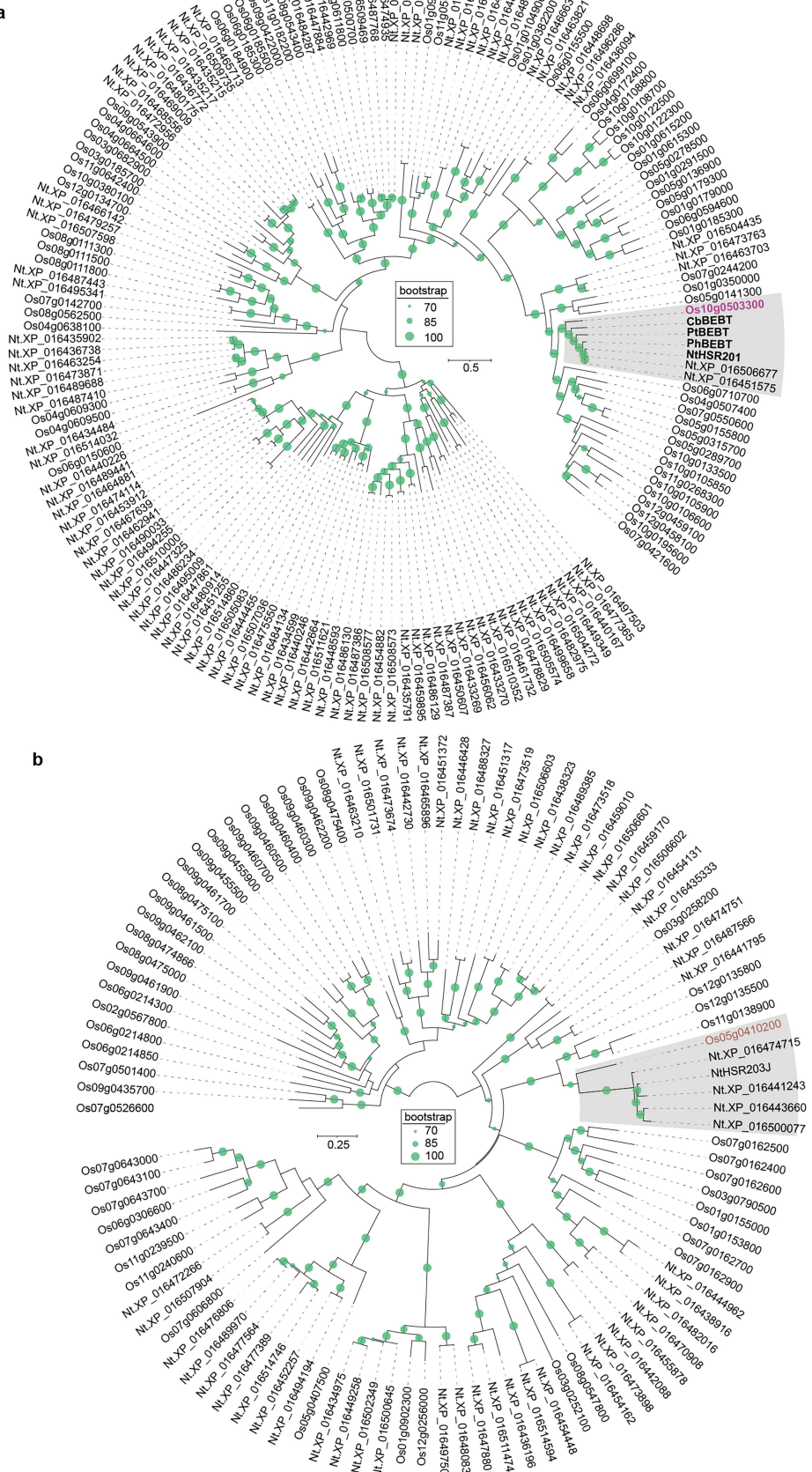
biosynthesis^{4,27,28,82–91}. (c) Summary of genetic studies examining the contribution of PAL and β-oxidation enzymes to SA biosynthesis in various plant species^{14,15,17,38,92,93}.



Extended Data Fig. 3 | Additional analysis of OsBEBT. (a) Sequence alignment of rice OsBEBT and other plant BEBT homologs. The amino acid sequence of rice OsBEBT was aligned with those of the putative orthologous proteins from other species, using the ClustalW sequence alignment program in MEGA7. Identical amino acids are highlighted in black, and similar amino acids are highlighted in gray. The conserved HXXXD and DFGWG motifs of the BAHD acyltransferase family are marked with yellow and pink boxes, respectively. Peroxisome targeting signal type 1 (PTS1) is indicated by a green box. (b) Analysis of purified His-tagged OsBEBT and OsBSE visualized by Coomassie-stained SDS-PAGE. For gel source data, see Supplementary Fig. 1. (c) For enzyme kinetics analysis of BA-CoA, the purified OsBEBT recombinant proteins were incubated with a saturated concentration of the indicated alcohols and varied concentrations of BA-CoA. Reaction products were quantified by UHPLC, and enzyme kinetic

parameters were derived by fitting the data to the Michaelis-Menten equation ($n=3$ independent experiments). ND, not detected. (d) *OsBEBT* mutation sites in *begt*. Inserted or deleted nucleotides are in red. Black box indicates exons, and light-gray boxes indicate the UTRs. (e) Developmental time course of SA accumulation in wild-type (ZH11) rice seedlings from germination to 30 days, sampled at five-day intervals. Data represent mean \pm SD ($n=3$ biologically independent samples). Statistical significance was determined by one-way ANOVA with post hoc Tukey HSD test. (f) SA accumulation in five-day-old rice leaves with or without benzylbenzoate treatment. Data represent mean \pm SD ($n=3$ biologically independent samples). Statistical significance was determined by Welch's ANOVA followed by Games-Howell post hoc tests. For e and f, SA contents were analyzed by LC-MS/MS with MRM and normalized to fresh weight.

Article



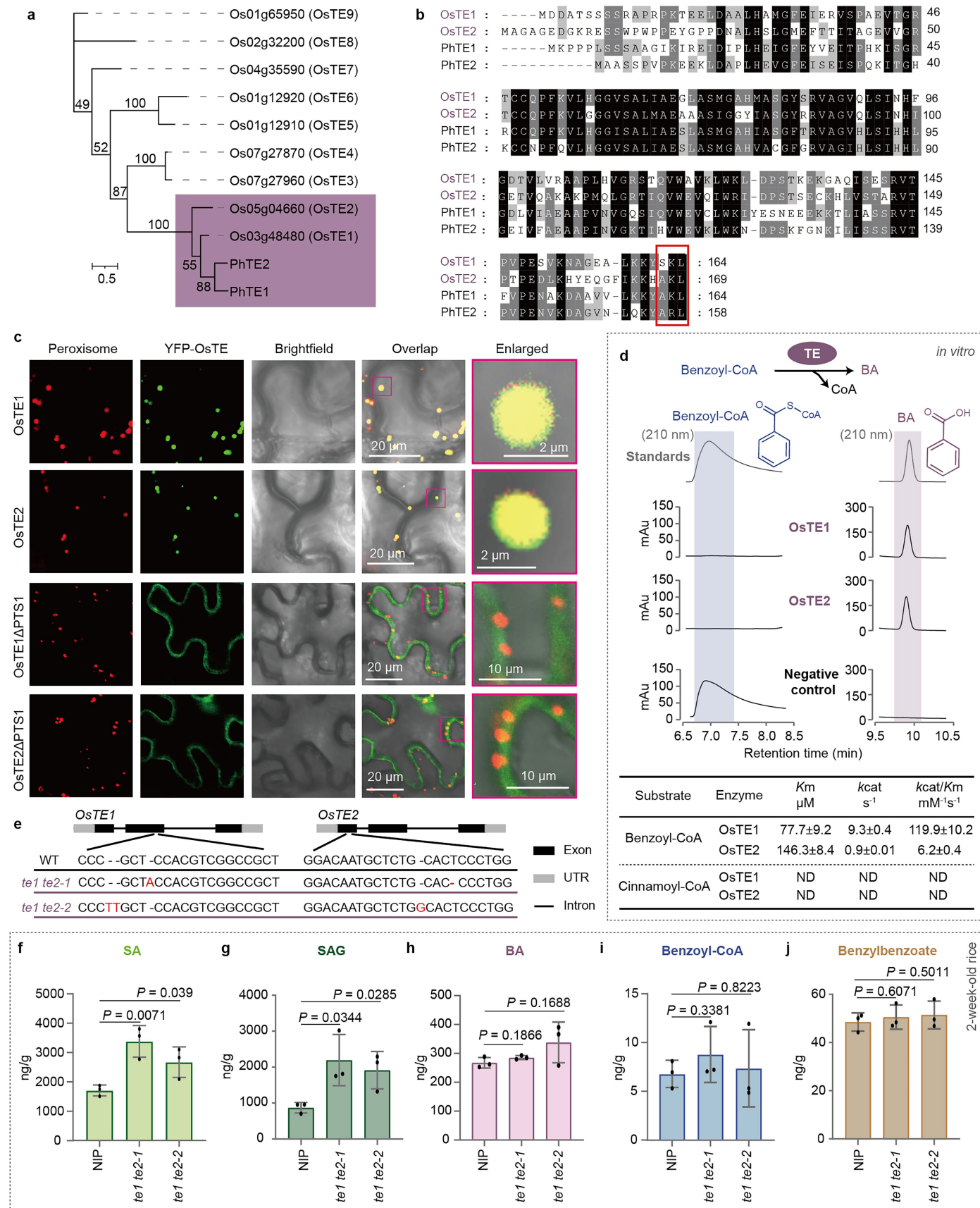
Extended Data Fig. 4 | See next page for caption.

Extended Data Fig. 4 | Phylogenetic analysis of OsBEBT and OsBSE.

(a) Phylogenetic analysis of Clade-V BAHD family proteins in rice and tobacco, together with CbBEBT, PtBEBT, and PhBEBT. All the known BEBT proteins are clustered in the same clade with Os10g0503300 (OsBEBT). (b) Phylogenetic

analysis of carboxyesterase (CXE) family proteins in rice and tobacco, including NtHSR203J. Among the rice proteins, Os05g0410200 is the closest to the tobacco branch containing NtHSR203J.

Article

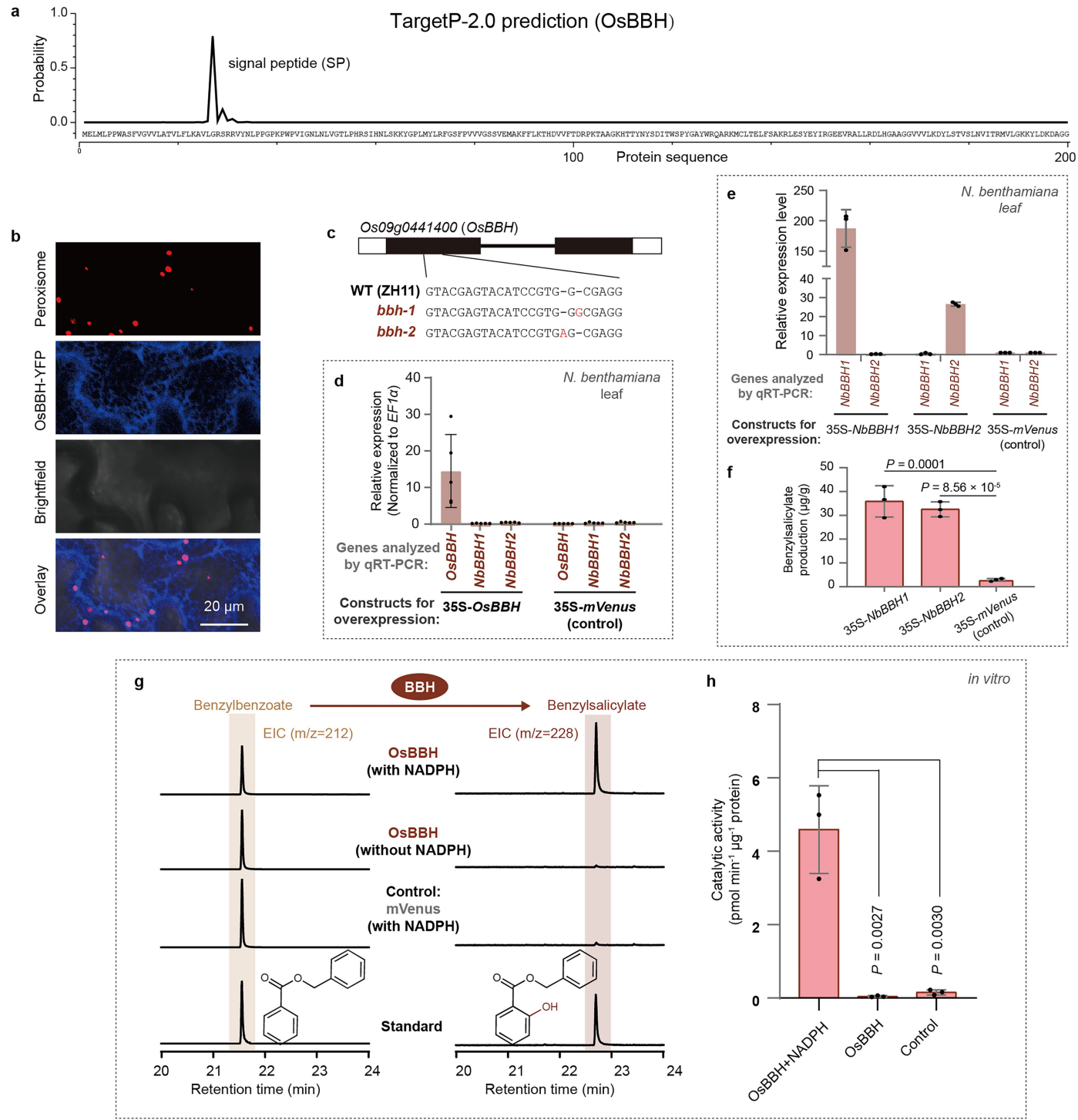


Extended Data Fig. 5 | See next page for caption.

Extended Data Fig. 5 | Characterization of OsTE1 and OsTE2. (a) Phylogenetic analysis of rice thioesterase (TE) family proteins and *Petunia hybrida* TE1 and TE2. (b) Sequence alignment of rice *Petunia hybrida* TE1 and TE2. The amino acid sequences of these TEs were aligned using the ClustalW sequence alignment program in MEGA7. Identical amino acids are highlighted in black, and similar amino acids are highlighted in gray. Peroxisome targeting signal type 1 (PTS1) is marked with a red box. (c) Subcellular localization of YFP-TEs. Confocal images are from tobacco leaf epidermis co-expressing the YFP-TEs and the peroxisomal marker CFP-SKL. OsTE1 Δ PTS1 indicates OsTE1 with its PTS1 tripeptide deleted. The magenta box enclosed area is enlarged and displayed. (d) Enzymatic characterization of OsTE proteins. Purified recombinant proteins were incubated with BA-CoA in enzymatic reactions, followed by HPLC analysis. Heat-inactivated protein served as a control. Chromatographs of

absorbance at wavelength 210 nm were displayed for substrates and products. For kinetics analysis, purified recombinant proteins were incubated with varying substrate concentrations, and the product was quantified by UHPLC. Kinetic parameters were analyzed using the Michaelis-Menten equation. Data represents mean \pm SD ($n = 3$ independent experiments). ND: not detected. (e) Mutation sites in the *OsTE1* and *OsTE2* genes in the mutants. Inserted nucleotides are in red. Black boxes indicate the exons, and light gray boxes indicate the UTRs. (f-j) Metabolite analysis of two-week-old wild-type and *te1 te2* mutant rice leaves. Levels of SA (f), SAG (g), BA (h), benzoyl-CoA (i), and benzylbenzoate (j) were quantified by LC-MS/MS-MRM and normalized to fresh weight. Data represents mean \pm SD ($n = 3$ biologically independent samples). Statistical significance was determined by two-tailed Student's *t*-tests.

Article

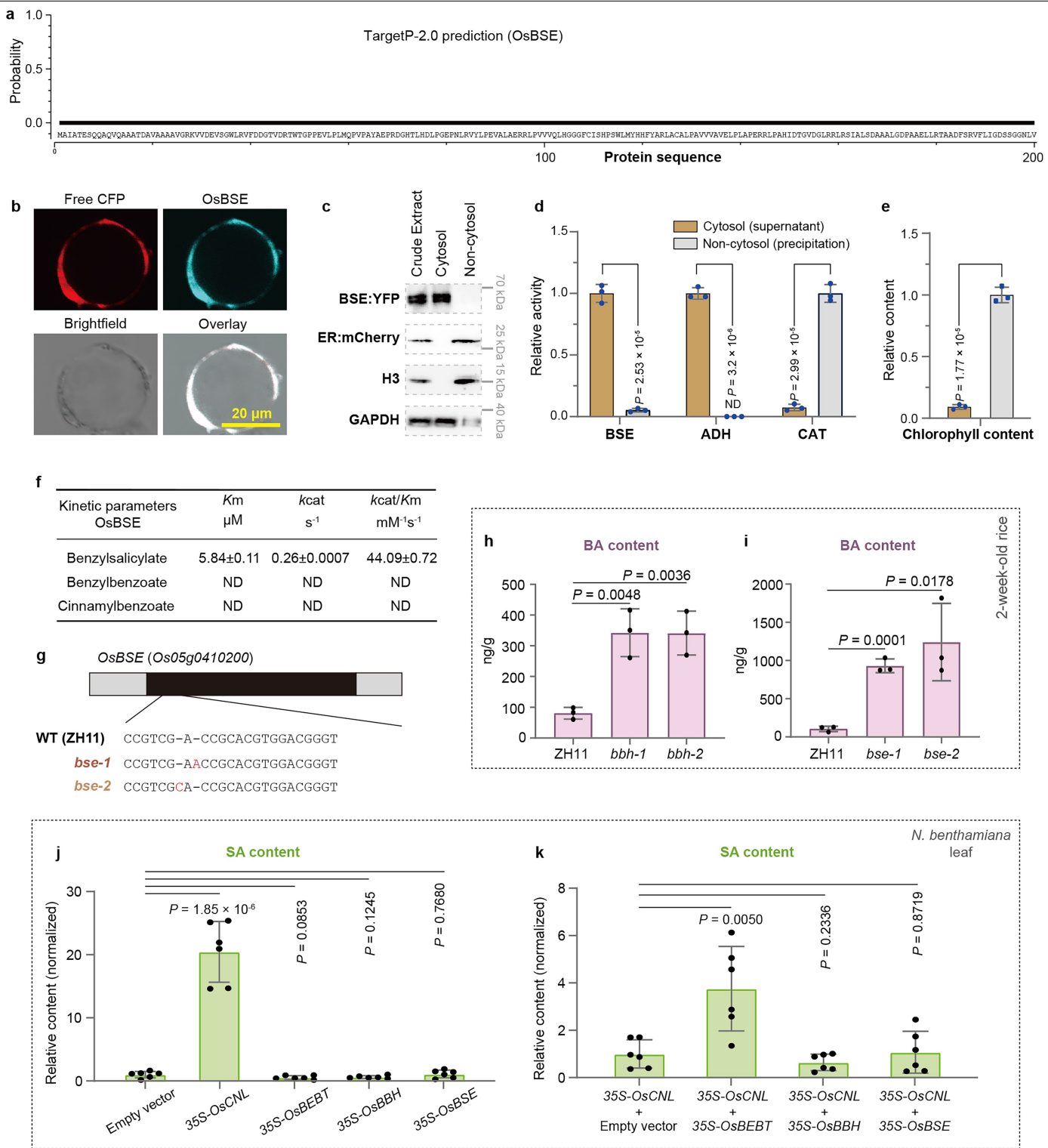


Extended Data Fig. 6 | See next page for caption.

Extended Data Fig. 6 | Additional characterization of OsBBH. (a) Signal peptide prediction for OsBBH using TargetP-2.0 (<https://services.healthtech.dtu.dk/services/TargetP-2.0/>). (b) Subcellular localization of OsBBH. Confocal images are from *N. benthamiana* leaf epidermis co-expressing YFP-OsBBH and the peroxisome marker CFP-SKL. (c) Mutation sites in rice *bbh* mutants. Inserted nucleotides are in red. Black boxes indicate the exons, light gray boxes indicate the UTRs, and the thick black line indicates the intron. (d) Gene expression levels of *OsBBH* and its *N. benthamiana* homologs (*NbBBH1* and *NbBBH2*) in leaves transiently expressing *OsBBH* or *mVenus* (control). Transcript levels were quantified by RT-qPCR relative to *NbEF1α* calculated by $2^{-\Delta Ct}$ value. Data represent mean \pm SD ($n = 5$ biologically independent samples). (e-f) Functional characterization of *NbBBH1* and *NbBBH2* in *N. benthamiana* using transient expression. (e) Gene expression analysis of *NbBBH1* and *NbBBH2* in transiently transformed leaves, where transcript levels were normalized to *mVenus* (control) samples using the $\Delta\Delta Ct$ method. (f) Quantification of

benzylsalicylate in leaves expressing *NbBBH1*, *NbBBH2*, or *mVenus* following treatment with benzylbenzoate. Products were analyzed by GC-MS using peak area of benzylsalicylate ($m/z = 228$) normalized to internal standard phenethyl phenylacetate ($m/z = 104$). The benzylsalicylate content was determined using standard curves generated from authentic standards. Data represent mean \pm SD ($n = 3$ biologically independent samples). Statistical significance was determined by two-tailed Student's *t*-tests. (g-h) In vitro enzymatic assays for OsBBH. Microsomes isolated from *N. benthamiana* leaves expressing *OsBBH* or *mVenus* (control) were incubated with benzylbenzoate with or without NADPH. (g) GC-MS analysis is shown with extracted ion chromatograms for benzylbenzoate ($m/z = 212$) and benzylsalicylate ($m/z = 228$). Peak intensities are shown relative to the highest signal for each compound. (h) OsBBH enzyme activity measured by quantifying the benzylsalicylate produced per μ g protein per minute. Data represent mean \pm SD ($n = 3$ independent experiments). Statistical significance was determined by two-tailed Student's *t*-tests.

Article

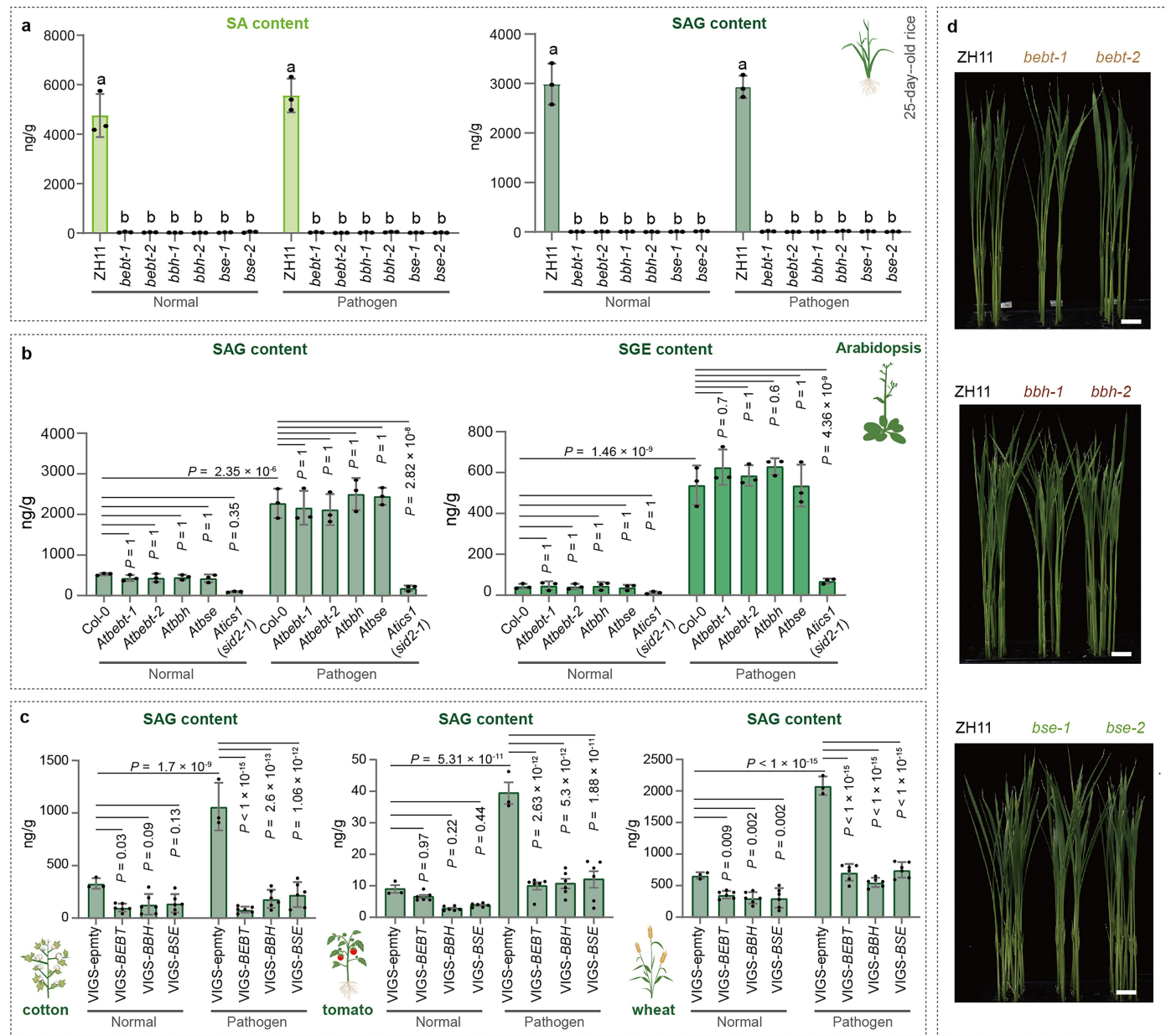


Extended Data Fig. 7 | See next page for caption.

Extended Data Fig. 7 | Additional characterization of OsBSE. (a) Signal peptide prediction for OsBSE using TatgetP-2.0. (b-c) Subcellular localization analysis of OsBSE. (b) Confocal images of rice protoplasts co-expressing the YFP-BSE and the free CFP as a cytosolic marker. (c) Immunoblot analysis of cytosolic and non-cytosolic fractions from rice protoplasts expressing OsBSE, with verification using organelle protein markers. For immunoblot source data, see Supplementary Fig. 1. (d-e) Subcellular distribution of BSE activity. Crude cell extracts of rice leaves were separated into cytosolic (supernatant) and non-cytosolic (precipitate) fractions by centrifugation. In (d), each fraction containing 5 µg protein was incubated with benzylsalicylate (500 µM), and BSE activity was determined by measuring SA production rate, normalized to the highest fraction activity. Fraction purity was verified using marker enzymes alcohol dehydrogenase (ADH, cytosolic marker) and catalase (CAT, peroxisomal marker) in (d), and chlorophyll content (chloroplast marker) in (e). Data represent mean ± SD ($n = 3$ independent experiments). Statistical significance was determined by two-tailed Student's *t*-tests. (f) For kinetics analysis, recombinant OsBSE proteins were incubated with varied concentrations of benzylsalicylate, benzylbenzoate or cinnamylbenzoate, and the corresponding products were quantified by UHPLC. Kinetic parameters were determined using the Michaelis-

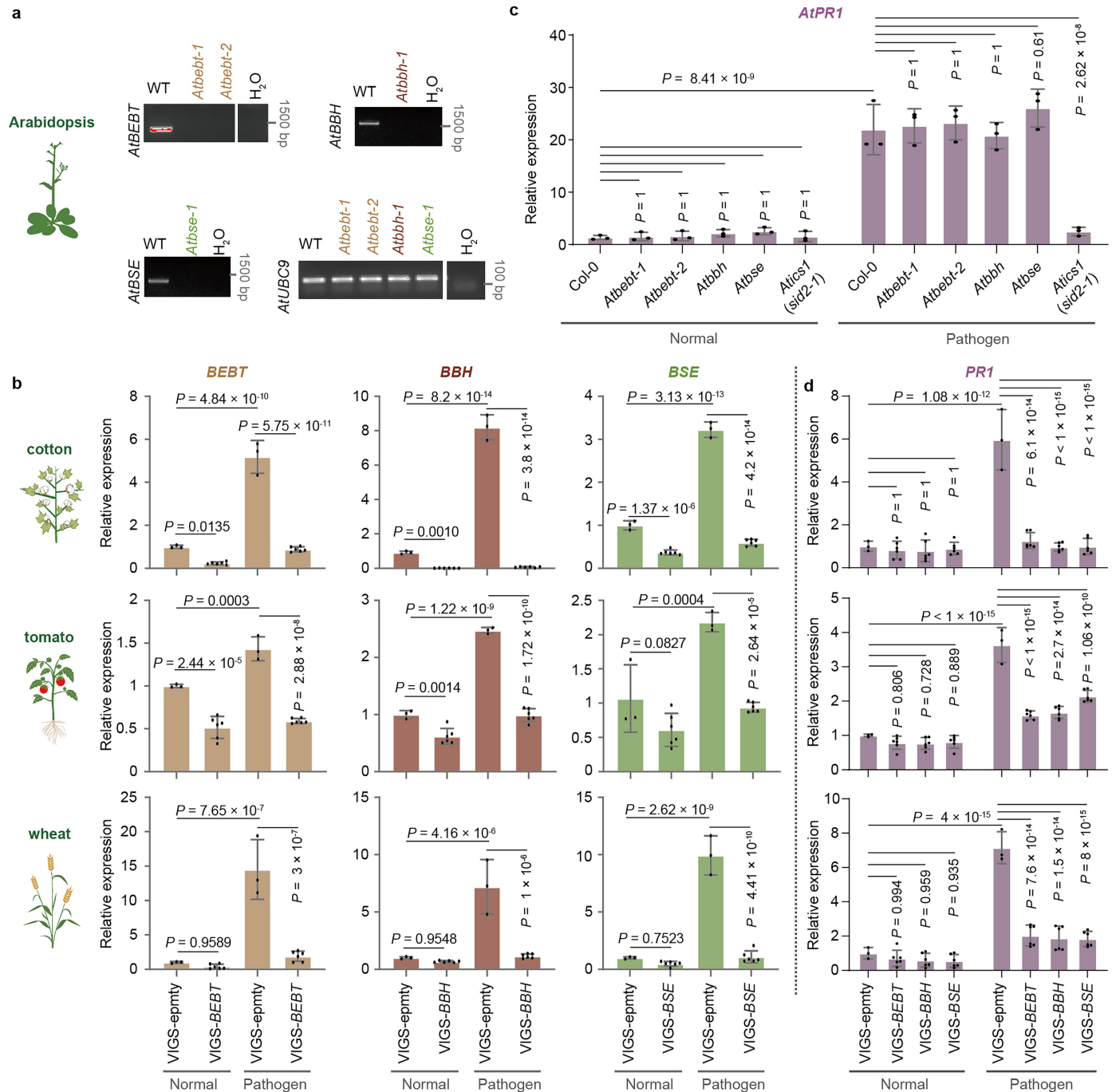
Menten model. Data represents mean ± SD ($n = 3$ independent experiments). ND, not detected. (g) Mutation sites in the *OsBSE* gene in the mutants. Inserted nucleotides are in red. Black box indicates the exon, and light gray boxes indicate the UTRs. (h-i) BA contents in 2-week-old *bbh* (h) and *bse* (i) rice mutants. BA was extracted from rice leaves and analyzed by LC-MS/MS-MRM. Data represent mean ± SD ($n = 3$ biologically independent samples). Statistical significance was determined by two-tailed Student's *t*-tests. (j) SA content in *N. benthamiana* plants transiently expressing *OsBEBT*, *OsBBH*, or *OsBSE*. Leaves were separately infiltrated with *Agrobacterium* carrying the empty vector, 35S-*OsCNL*, 35S-*OsBEBT*, 35S-*OsBBH*, or 35S-*OsBSE*. SA content was analyzed 2 days post-infiltration. Data represent mean ± SD ($n = 6$ biologically independent samples). Statistical significance was determined by two-tailed Student's *t*-tests. (k) SA contents in *N. benthamiana* leaves co-expressing *OsCNL* with *OsBEBT*, *OsBBH*, or *OsBSE*. Equal amounts of *Agrobacterium* carrying 35S-*OsCNL* were co-infiltrated with strains containing the empty vector, 35S-*OsBEBT*, 35S-*OsBBH*, or 35S-*OsBSE*. SA content was analyzed 2 d post-infiltration. Data represent mean ± SD ($n = 6$ biologically independent samples). Statistical significance was determined by two-tailed Student's *t*-tests.

Article



Extended Data Fig. 8 | Measurement of SA, SAG, and SGE levels in multiple plant species under different pathogen challenges. (a) SA and SAG contents in 25-day-old *bbe*, *bbh* and *bse* rice mutants with or without *M. oryzae* (strain RB22) infection. Data represent mean \pm SD ($n = 3$ biologically independent samples). Different letters indicate significant differences ($P < 0.05$) determined by one-way ANOVA with post hoc Tukey HSD test. (b) SAG and SGE contents in 30-day-old *bbe*, *bbh*, *bse*, and *ics* Arabidopsis mutants with or without *Pseudomonas syringae* DC3000 infection. Data represent mean \pm SD ($n = 3$ biologically independent samples). Statistical significance was determined by one-way ANOVA with post hoc Tukey HSD test. (c) SAG content in VIGS-silenced plants following pathogen infection. Plants were individually silenced for *BEBT*, *BBH*, or *BSE* homologs using VIGS. Gene accessions are described in the Methods. SAG quantification was performed under both control and pathogen-infected conditions for cotton infected with *Verticillium dahliae* V991, tomato infected with *P. syringae* DC3000, and wheat infected with *Fusarium graminearum*. Data represents mean \pm SD (control: $n = 3$ biologically independent samples; VIGS-treated: $n = 6$ biologically independent samples). Statistical significance was determined by one-way ANOVA with post hoc Tukey HSD test.

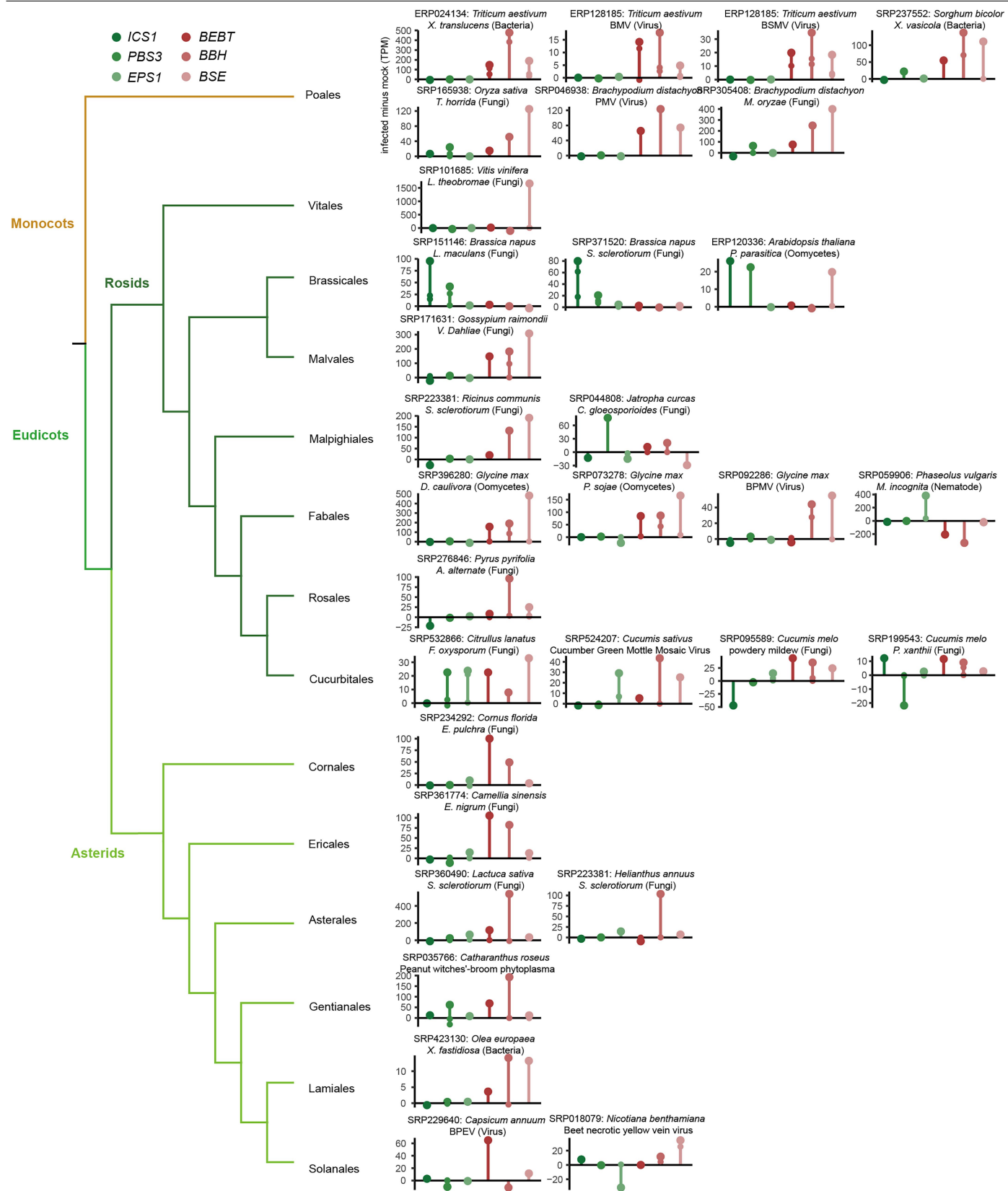
(d) Representative images of 20-day-old rice mutants (*bbe*, *bbh*, and *bse*) showing normal growth phenotypes compared with wild type (ZH11). Scale bar: 1.5 cm. For a-c, SA, SAG and SGE were quantified by LC-MS/MS-MRM and normalized to fresh weight.



Extended Data Fig. 9 | Gene expression analysis of SA biosynthetic and responsive genes in mutant and gene-silenced plants. (a) Semi-quantitative RT-PCR analysis of *BEBT*, *BBH*, and *BSE* homologs in *Arabidopsis* mutants. *AtUBC9* served as the reference gene. RNA was extracted from leaves and reverse-transcribed for analysis. For gel source data, see Supplementary Fig. 1. (b) RT-qPCR analysis of the expression of *BEBT*, *BBH*, and *BSE* homologs in VIGS-treated tomato, wheat, and cotton plants with or without pathogen infection. Data represent mean ± SD (control: $n = 3$ biologically independent samples; VIGS groups: $n = 6$ biologically independent samples). Statistical significance was determined by one-way ANOVA with post hoc Tukey HSD test.

(c) RT-qPCR analysis of the expression of *PR1* in 30-day-old *bebt*, *bbh*, *bse*, and *ics* *Arabidopsis* mutants with or without pathogen infection. Data represent mean ± SD ($n = 3$ biologically independent samples). Statistical significance was determined by one-way ANOVA with post hoc Tukey HSD test. (d) RT-qPCR analysis of the expression of *PR1* in VIGS-treated tomato, wheat, and cotton plants. Data represent mean ± SD (control: $n = 3$ biologically independent samples; VIGS groups: $n = 6$ biologically independent samples). Statistical significance was determined by one-way ANOVA with post hoc Tukey HSD test.

Article



Extended Data Fig. 10 | Pathogen-induced expression pattern of genes involved in the two SA biosynthetic routes in diverse plants (representing 25 species from 15 orders). In each lollipop plot, the isochorismate- and phenylalanine-derived routes are colored by green (dark to light) and red (dark to light), respectively. The top three homologous genes with the highest absolute difference relative expression level (infected vs. mock) are shown.

The transcriptome data of infected and mock plants are publicly available at NCBI's Sequence Read Archive (SRA) Browser (<https://www.ncbi.nlm.nih.gov/sra>). Trim Galore v 0.6.10 removed low-quality reads and adapter sequences. Clean reads were mapped to the reference genome using STAR v 2.7.10b, and featureCounts v2.0.6 was used to count reads per gene. Gene expression quantification was performed using the TPM (Transcripts Per Million) values.

Reporting Summary

Nature Portfolio wishes to improve the reproducibility of the work that we publish. This form provides structure for consistency and transparency in reporting. For further information on Nature Portfolio policies, see our [Editorial Policies](#) and the [Editorial Policy Checklist](#).

Statistics

For all statistical analyses, confirm that the following items are present in the figure legend, table legend, main text, or Methods section.

n/a Confirmed

- The exact sample size (n) for each experimental group/condition, given as a discrete number and unit of measurement
- A statement on whether measurements were taken from distinct samples or whether the same sample was measured repeatedly
- The statistical test(s) used AND whether they are one- or two-sided
Only common tests should be described solely by name; describe more complex techniques in the Methods section.
- A description of all covariates tested
- A description of any assumptions or corrections, such as tests of normality and adjustment for multiple comparisons
- A full description of the statistical parameters including central tendency (e.g. means) or other basic estimates (e.g. regression coefficient) AND variation (e.g. standard deviation) or associated estimates of uncertainty (e.g. confidence intervals)
- For null hypothesis testing, the test statistic (e.g. F , t , r) with confidence intervals, effect sizes, degrees of freedom and P value noted
Give P values as exact values whenever suitable.
- For Bayesian analysis, information on the choice of priors and Markov chain Monte Carlo settings
- For hierarchical and complex designs, identification of the appropriate level for tests and full reporting of outcomes
- Estimates of effect sizes (e.g. Cohen's d , Pearson's r), indicating how they were calculated

Our web collection on [statistics for biologists](#) contains articles on many of the points above.

Software and code

Policy information about [availability of computer code](#)

Data collection

- 1.Qualitative characterization of enzyme activity was performed using HPLC (Shimadzu LC-20A, Japan) equipped with a photodiode array (PDA) detector set at 210 nm. Enzyme kinetics were measured using a UHPLC system (Vanquish Flex, Thermo Fisher Scientific, USA) with either a variable wavelength detector (VWD) or a fluorescence detector (FLD).
- 2.Analysis of SA and related compounds was conducted using an ExionLC HPLC system coupled with an AB SCIEX QTRAP 6500plus mass spectrometer, as well as an Agilent GC 8890 gas chromatograph equipped with a 5977B detector.
- 3.Fluorescence signals were detected using an Olympus FV3000 confocal microscope.
- 4.RT-qPCR was performed on a LightCycler 480 II instrument (Roche).
- 5.Absorbance measurements were obtained using a Synergy H1 microplate reader (BioTek/Agilent, USA).
- 6.Immunoblot images were acquired using a Tanon-5200 Chemiluminescent Imaging System (Tanon Science & Technology, China).

Data analysis

- 1.GC-MS analysis: Data were processed using Agilent MassHunter Qualitative Analysis software (version B.08.00).
- 2.LC-MS/MS analysis: Data were analyzed with Agilent MassHunter Quantitative Analysis software (version 10.0).
- 3.Sequence analysis: Sequence data were analyzed using SnapGene (version 6.0.2).
- 4.Phylogenetic analysis: Phylogenetic trees were constructed using IQ-TREE (version 2.3.0), with sequence alignments generated by MAFFT (v7.490), protein homology searches performed with DIAMOND (v2.0.14), and alignments trimmed using TrimAl (v1.4).
- 5.Statistical analysis: Statistical analyses were conducted using GraphPad Prism 8.
- 6.Gene co-expression visualization: Gene co-expression networks were visualized using Cytoscape (version 3.7.2).
- 7.Transcriptomic gene expression analysis: Transcriptome data were processed using Trim Galore (v0.6.10), STAR (v2.7.10b), and featureCounts (v2.0.6).
- 8.Protein sequence alignment: The amino acid sequence of rice OsBEBT was aligned with putative orthologs from other species using ClustalW in MEGA7.

9. Leaf lesion area quantification: The area of leaf lesions used for quantifying disease symptoms was measured using ImageJ software (version 1.42q).

For manuscripts utilizing custom algorithms or software that are central to the research but not yet described in published literature, software must be made available to editors and reviewers. We strongly encourage code deposition in a community repository (e.g. GitHub). See the Nature Portfolio [guidelines for submitting code & software](#) for further information.

Data

Policy information about [availability of data](#)

All manuscripts must include a [data availability statement](#). This statement should provide the following information, where applicable:

- Accession codes, unique identifiers, or web links for publicly available datasets
- A description of any restrictions on data availability
- For clinical datasets or third party data, please ensure that the statement adheres to our [policy](#)

All data associated with this study are provided. The full version of all images of gels and immunoblots are provided in the Supplementary Figure 1. The accession numbers of all genes cloned or experimentally analyzed in this study are shown in the Supplementary Tables 1 & 2. Sequence data related to these genes can be found in the GenBank/EMBL data libraries. Gene co-expression data can be accessed from the ATTED-II database (https://atted.jp/top_search/#CoExSearch) and are also provided within the Source Data file. The source data behind all graphs are available in the Source Data files. The gene expression data presented in Extended Data Figure 10 can be obtained from the NCBI Sequence Read Archive (SRA) database (<https://www.ncbi.nlm.nih.gov/sra>) using the BioProject accession number indicated in the figure, and are also provided in the source data.

Research involving human participants, their data, or biological material

Policy information about studies with [human participants or human data](#). See also policy information about [sex, gender \(identity/presentation\), and sexual orientation](#) and [race, ethnicity and racism](#).

Reporting on sex and gender This information has not been collected

Reporting on race, ethnicity, or other socially relevant groupings This information has not been collected

Population characteristics This information has not been collected

Recruitment This information has not been collected

Ethics oversight This information has not been collected

Note that full information on the approval of the study protocol must also be provided in the manuscript.

Field-specific reporting

Please select the one below that is the best fit for your research. If you are not sure, read the appropriate sections before making your selection.

Life sciences Behavioural & social sciences Ecological, evolutionary & environmental sciences

For a reference copy of the document with all sections, see nature.com/documents/nr-reporting-summary-flat.pdf

Life sciences study design

All studies must disclose on these points even when the disclosure is negative.

Sample size	Most experiments were performed with three biological replicates, which is the minimum number required for robust statistical analysis of metabolite data and sufficient to assess experimental variability. For specialized experiments, such as VIGS and tobacco transient expression, three to six replicates were used to ensure the reliability of the results.
Data exclusions	No data was excluded
Replication	All experiments were successfully repeated at least three times, and the number of independent experiments or biological replicates is indicated in the figure legends. For immunoblot, fluorescent microscope, and semiquantitative RT-PCR analyses, representative images are shown and described in "Statistical analysis and reproducibility" in Method section.
Randomization	Allocation was random
Blinding	This experiment does not involve blinding because there is no subjective allocation involved in this study.

Reporting for specific materials, systems and methods

We require information from authors about some types of materials, experimental systems and methods used in many studies. Here, indicate whether each material, system or method listed is relevant to your study. If you are not sure if a list item applies to your research, read the appropriate section before selecting a response.

Materials & experimental systems		Methods	
n/a	Involved in the study	n/a	Involved in the study
<input type="checkbox"/>	<input checked="" type="checkbox"/> Antibodies	<input checked="" type="checkbox"/>	<input type="checkbox"/> ChIP-seq
<input checked="" type="checkbox"/>	<input type="checkbox"/> Eukaryotic cell lines	<input checked="" type="checkbox"/>	<input type="checkbox"/> Flow cytometry
<input checked="" type="checkbox"/>	<input type="checkbox"/> Palaeontology and archaeology	<input checked="" type="checkbox"/>	<input type="checkbox"/> MRI-based neuroimaging
<input checked="" type="checkbox"/>	<input type="checkbox"/> Animals and other organisms		
<input checked="" type="checkbox"/>	<input type="checkbox"/> Clinical data		
<input checked="" type="checkbox"/>	<input type="checkbox"/> Dual use research of concern		
<input type="checkbox"/>	<input checked="" type="checkbox"/> Plants		

Antibodies

Antibodies used

anti-Histone H3 (Cat# ab1791, Abcam), anti-GAPDH (Cat# HRP-60004, Proteintech), anti-YFP/GFP (Cat# E-A02020, Abbkine), and anti-mCherry/RFP (Cat# ab65856, Abcam)

Validation

The anti-Histone H3 (Cat# ab1791, Abcam) is verified as described in website (<https://www.abcam.cn/products/primary-antibodies/histone-h3-antibody-nuclear-marker-and-chip-grade-ab1791.html>); the anti-GAPDH (Cat# HRP-60004, Proteintech) is verified as described in website (<https://www.ptgn.com/products/GAPDH-Antibody-60004-1-PBS.htm>); anti-YFP/GFP (Cat# E-A02020, Abbkine) is verified as described in website (<https://www.abbkine.com/datasheet/A02020.pdf>); the anti-mCherry/RFP (Cat# ab65856, Abcam) is verified as described in website (<https://www.abcam.cn/products/primary-antibodies/mcherry-antibody-ab167453.html>)

Dual use research of concern

Policy information about [dual use research of concern](#)

Hazards

Could the accidental, deliberate or reckless misuse of agents or technologies generated in the work, or the application of information presented in the manuscript, pose a threat to:

No	Yes
<input checked="" type="checkbox"/>	<input type="checkbox"/> Public health
<input checked="" type="checkbox"/>	<input type="checkbox"/> National security
<input checked="" type="checkbox"/>	<input type="checkbox"/> Crops and/or livestock
<input checked="" type="checkbox"/>	<input type="checkbox"/> Ecosystems
<input checked="" type="checkbox"/>	<input type="checkbox"/> Any other significant area

Experiments of concern

Does the work involve any of these experiments of concern:

No	Yes
<input checked="" type="checkbox"/>	<input type="checkbox"/> Demonstrate how to render a vaccine ineffective
<input checked="" type="checkbox"/>	<input type="checkbox"/> Confer resistance to therapeutically useful antibiotics or antiviral agents
<input checked="" type="checkbox"/>	<input type="checkbox"/> Enhance the virulence of a pathogen or render a nonpathogen virulent
<input checked="" type="checkbox"/>	<input type="checkbox"/> Increase transmissibility of a pathogen
<input checked="" type="checkbox"/>	<input type="checkbox"/> Alter the host range of a pathogen
<input checked="" type="checkbox"/>	<input type="checkbox"/> Enable evasion of diagnostic/detection modalities
<input checked="" type="checkbox"/>	<input type="checkbox"/> Enable the weaponization of a biological agent or toxin
<input checked="" type="checkbox"/>	<input type="checkbox"/> Any other potentially harmful combination of experiments and agents

Plants

Seed stocks

The plant materials used in this study consisted of: (1) rice (*Oryza sativa*) wild-type cultivars ZH11 and NIP maintained in our laboratory; (2) rice cnl mutant from our previous study (DOI: 10.1016/j.devcel.2024.03.023); (3) rice bebt, bbh, and bse mutants generated via CRISPR/Cas9 by Biogle Genetech (<http://www.biogle.cn>); (4) rice te1 te2 double mutants created using CRISPR/Cas9, CRISPR/Cas9-mediated gene editing was employed to generate knock-out lines, harboring mutations in PEP1, (Oryzopsis rufipila), TEF2, and DPFSE genes obtained from Prof. Xin Xiufang (Center for Excellence in Molecular Plant Sciences, Chinese Academy of Sciences); and (7) Arabidopsis T-DNA insertion mutants Atbebt-1 (SALK_030095), Atbebt-2 (SALK_089260), Atbse (SALK_205911), and Atbbh (SALK_039417) from the SALK collection (<https://abrc.osu.edu/>).

Novel plant genotypes

The rice bebt, bbh, te1 te2, and bse mutants were genotyped by PCR using primers listed in Supplementary Table 2. Mutation sites were verified by sequencing and analyzed with SnapGene software (<https://www.snapgene.com>). For Arabidopsis, the Atbebt, Atbbh, and Atbse mutants were verified by RT-PCR analysis.